DESIGN AND EXPERIMENTATION OF A TUNABLY COMPLIANT ROBOTIC FINGER USING LOW MELTING POINT METALS

by

HEON JOO

A thesis submitted in partial fulfillment of
the requirements for the degree of

MASTER OF SCIENCE IN MECHANICAL ENGINEERING

WASHINGTON STATE UNIVERSITY
Department of Mechanical and Materials Engineering

JULY 2017

To the Faculty of Washington State University:

The members of the Committee appointed to examine the thesis of HEON JOO find it satisfactory and recommend that it be accepted.

John Swensen, Ph.D., Chair

Arda Gozen, Ph.D.

Matthew Taylor, Ph.D.

ACKNOWLEDGMENTS

I would like to thank my advisor, Dr.Swensen who has taught and guided so far for this thesis completion and also thank Dr.Taylor for joining me in his project. During the last two years, my wife sincerely supported me with a lot of courage and hope and my son was another delight that made me endure here to the end. I would like to express my deepest gratitude to all of the families in Korea, especially my grandmother. She is the most appreciated and precious person in my life that made me today. Also, I would like to appreciate many Koreans we have known in Pullman. Lastly, I would like to give my infinite glory and gratitude to God who gave me and my family the strength, courage, and wisdom to overcome any difficulties.

DESIGN AND EXPERIMENTATION OF A TUNABLY

COMPLIANT ROBOTIC FINGER USING

LOW MELTING POINT METALS

Abstract

by Heon Joo, M.S.
Washington State University
July 2017

Chair: John Swensen

In this thesis, it is explaining that the fabrication and testing of a tunably-compliant tendon-driven finger implemented through the geometric design of a skeleton made of the low-melting point Field's metal encased in a silicone rubber. The initial prototype consists of a skeleton comprised of two rods of the metal, with heating elements in thermal contact with the metal at various points along its length, embedded in an elastomer. The inputs to the systems are both the force exerted on the tendon to bend the finger and the heat introduced to liquefy the metal locally or globally along the length of the finger. Selective localized heating allows multiple joints to be created along the length of the finger.

Fabrication was accomplished via a multiple step process of elastomer casting and liquid metal casting. Heating elements such as power resistors or Ni-Cr wire with electrical connections were added as an intermediate step before the final elastomer casting. The addition of a tradition tendon actuation was inserted after all casting steps had been completed. While preliminary, this combination of selective heating and engineered geometry of the low-melting point skeletal structure will allow for further investigation into the skeletal geometry and its effects on local and global changes in device stiffness.

TABLE OF CONTENTS

LIST OF TABLES

LIST OF FIGURES

Dedication

This thesis is dedicated to my grandmother, Youngja Choi who has given huge endeavor and all sacrifices for me throughout her lifetime and to my aunt, Youngsook Joo who loved and cared me greatly. Also, I dedicate this thesis to the companion of my life, Hyojeong Byeon, and my lovely son, Sihwan Joo, and all of the families in my home country. I am very grateful to the God about this work.

CHAPTER 1. INTRODUCTION

In 2011, the U.S. National Science Foundation announced an ongoing effort entitled the National Robotics Initiative, whose primary objective is to "develop robots that work with or beside people to extend or augment human capabilities, taking advantage of the different strengths of humans and robots." This emphasis on humans and robots working the same environments – a component of what has come to be known as co-robotics – has increased research interest in the area of soft robotics. The early research in this area of soft robots has tended to be made wholly of soft elastomers and actuation using either tendons or compressed air. One of the key limitations of the current state of the art in soft robotics is that, while able to safely interact with human collaborators, their inherent high degree of compliance limits the degree to which they can interact with their environment. They have limited ability to exert forces and conduct manipulations on their surrounding environment because of their inherent high degree of compliance.

Thus, a principal aim of the proposed work is to create a new type of compliant robotics, where the robotic materials and structure can switch between acting as a traditional rigid robotic design and the new class of soft robotic designs. Though only discussed on a macroscopic scale in this thesis, the eventual goal is compliant devices

that change their stiffness in a broad range of spatiotemporal scales. In general, it is somewhat complicated and difficult to design and fabricate a robotic finger with this kind of tunable stiffness using traditional methods. Mechanical structures comprised of components such as motors, linkages, and gears can be used to create a structure capable of retaining specific shapes, but their use increases the system's complexity, and they are generally not capable of producing complex and continuous deformations [1]. However, by using smart materials, such as the low melting point Field's metal, embedded in elastomers and other soft-robotic materials, it becomes easier to fabricate soft robotic components that exhibit this tunable behavior. Field's metal or Field's alloy is a fusible alloy that becomes liquid at approximately 62 °C (144 °F) [2]. It is a eutectic alloy that the solid and liquid temperatures are the same and composed of bismuth, indium, and tin with the following percentages by weight: 32.5% Bi, 51% In, 16.5% Sn [2].

A standard approach to soft robotics has been the construction of components made entirely of silicone with fluid-filled cavities for sensing and actuation. This silicone body approach has helped to shape the idea of a truly "soft" robot since most of the body is formed out of a soft, elastomeric material with an extremely low stiffness [3, 4]. Many of the silicone elastomers used in soft robotics are capable of sustaining its strain anywhere from 100-500% rate of high deformation [3, 4]. This soft elastomer silicone is used to wrap up the Field's metal shaped like a long rod and

the Ni-Cr wires comprise layers above and below the metal skeleton. When electric current flows through the Ni-Cr wire, and it becomes hot, the temperature will go up to the point of melting the Field's metal inside the silicone. When the metal inside melts, the silicone can be bent with the metal rods like bending a finger. Elastomers with electrically controlled stiffness have the potential to revolutionize robotics and assistive wearable technologies by allowing actuators to independently and reversibly change both their shape and elastic rigidity [5]. Many variable stiffness actuators require complicated design a machining to achieve a change of stiffness in even a single degree of freedom [6, 7, 8]. However, the approach using a low melting temperature metal alloy provides new ideas, for instance, the latch-able microvalve is able to stay closed or open from the different state of the metal alloy by the temperature. The approach with the low melting point metal alloy also can make the elastic rigidity of soft elastomer tunable by the electrically controlled heating element [2, 5].

In this thesis, we deal with an initial device design with two rods of low melting point Field's metal alloy as a skeleton, Ni-Cr wire, and power resistors as a heater and thermocouples to track the internal heating and cooling of the compliant device. All materials are embedded in a silicone rubber and the whole device can be actuated by the tendon routed on the top surface when the state of metal rods are changed by the temperature. These could be a building block for many soft robotic structures, but we pose the problem as the core of a tunably-compliant robotic finger. The primary

contribution is an investigation of the ability to bias the temperature of the compliant device to near the melting point of the metal and then observing the rate at which the mechanism can switch between its stiff and compliant regimes.

CHAPTER 2. RELATED WORK

Animals exploit soft structures to move effectively in complex natural environments. These capabilities have inspired robotic engineers to incorporate soft technologies into their designs [9, 10]. For example, elephant's nose is analogous to their hand. They can freely move their long nose's muscles to move to the desired position, and the shape of the tip is similar to the hand that can naturally grab things. The nose of the elephant evokes the desire of robot researchers to create robotic arms and hands that are perfectly similar. As early work in the field of biomimetic long dexterous robots, Walker and Hannan developed a novel hyper-redundant robot manipulator which featured a backbone of 32 degrees of freedom, with 8 independently driven tendons to achieve motion and shape adaptation capabilities similar to an elephant [11, 12]. Actuation is provided via a series of tendons routed through the structure. In function, the manipulator has capabilities similar to that of the trunk of an elephant, with the ability to bend into numerous shapes and conform easily to the environment [11, 12]. For the hardware design, they designed each segment which can serve as a method for routing the cables. With the series combination of the segments can give the manipulator its defining shapes. The overall motion of the manipulator is controlled by a tendon (cable) servo system [11]. The idea inspired by the motion

of the elephant nose was analogously able to be feasible by using a noble design of continuous circular segments that can be connected to the tendon and the motor that manipulates each tendon for the nose's locomotion. Other biomimetic approaches to soft robotics have used squid, starfish, worms, and other cephalopods as inspiration [13, 14, 15]. "Multi-gait Soft Robot" was composed exclusively of soft materials like elastomeric polymers. Soft lithography was used to fabricate a pneumatically actuated robot capable of sophisticated locomotion, for example, fluid movement of limbs and multiple gaits. This robot is quadrupedal and it uses no sensors but only five actuators with a simple pneumatic valving system that operates at low pressures below $10psi$. A combination of crawling and undulation gaits allowed this robot to navigate a difficult obstacle [13].

In addition to the robots that imitate the movement of soft animals, there have been many studies to make the motions of human beings surrounded by soft skin and muscles to the robotic devices. In particular, the materials such as silicone elastomer have been mainly used, which can soften and adjust the stiffness in various ways, without using the existing conventional hard materials, to make this kind of grippers which can imitate the human hand and pick up something. "Monolithic Fabrication of Sensors and Actuators in a Soft Robotic Gripper" is a fluidically functionalized soft-bodied robot that integrates both sensing and actuation [4]. There are two specific designed molds to cast the robot. The primary one, initially filled with

the liquid elastomer, with an inset showing the embossed channels that create the sensor channels. Another one is the channel mold that is placed in the primary mold to create the pneumatic channels in the robot [4]. Briefly speaking about the fabrication, the bottom half of the mold is printed and filled with liquid elastomer. The channel mold is embedded inside the liquid elastomer to create the pneumatic channels. When the elastomer has cured, the mold can be removed from around it. To finish the sensors, the channels are filled with liquid metal (eutectic Indium Gallium alloy: eGaIn) and sealed with the liquid elastomer. Finally, the pneumatic channels are sealed by bonding the body to a thin layer of "Silgard 184" and they attached it to a compressed air source with a flow valve control system that limited the gauge pressure to activate the robot [4].

The field of soft robotics has been an ideal platform for the applications of smart materials actuators and multi-functional materials that incorporate both sensing and actuation [4]. Much of this research takes inspiration from nature in attempts to imitate the movement of soft animals. In particular, materials such as silicone elastomers have been used extensively, either as a complete soft robotic device or as an outer skin on conventional hard materials. A primary method of actuation in soft robotics has been pneumatic chambers and channels [10, 14, 15, 16, 17]. However, alternative approaches have employed combinations of multiple smart materials, such as shape memory alloys, shape memory polymers, or low-melting point metals [5, 18]. The

prior state of the art in tunable compliance was traditional variable stiffness actuators with tunable series elastic components. These variable stiffness actuators often require complicated design, machining, and fabrication to achieve a change of stiffness in even a single degree of freedom [6, 7, 8, 19, 20, 21]. The proposed approach, similar to Shaikh [2] and Wanliang [5], takes a different approach of using smart materials as aggregates in a soft robotic composite but extends the work to include axis-level control of the stiffness changes. They used a phase-changing metal alloy to reversibly tune the elastic rigidity of an elastomer composite. The elastomer is embedded with a sheet of low-melting-point Field's metal and an electric Joule heater composed of a serpentine channel of liquid-phase gallium-indium-tin alloy. At room temperature, the embedded Field's metal is solid and the composite remains elastically rigid. Joule heating causes the Field's metal to melt and allows the surrounding elastomer to freely stretch and bend [5]. The composite was configured three layers that the top layer is the elastomer sealing layer, the middle one is the liquid–phase Joule heating element, and the bottom layer is the thermally activated layer of Field's metal. When electrically activated, the composite softens and easily deforms. The stiffness of composite can be tunable with Field's metal strip and by the liquid-phase Galinstan heater.

Soft robots have many potentials with various ideas and inspirations compared to the conventional rigid robots. If the development of robots that can move as

smoothly as the gestures of human beings or natural animals can be made using soft materials and properties of various materials, this may be a big step forward in robot research and development. In this regard, the proposed approach in this thesis suggests the better method how to create the joints using heaters at the certain positions of the low melting point metal alloy and also how to switch the rigid and soft states temporally and spatially. Although the proposed approach better than the methods of conventional soft robots, there will still be a room for further study in my research which aims to make the diverse type of robots or devices using the low melting point metal as a core component.

CHAPTER 3. DESIGN AND FABRICATION

The device was designed for the shape of the human finger. For example, it is similar in terms of the geometrical features, a tendon like wire actuation mechanism, and the use of soft materials for achieving passive adaptability [22]. For the geometry of this finger design as seen in Figure 3.1, the length was twice that of an average adult's finger with a rectangular shape, and the thickness was supposed to be as thin as possible to facilitate bending when compliant. We used two metal rods side by side with approximately 10-11mm gap such that the device is compliant in torsion and stiff in bending even when the metal is in the solid state.

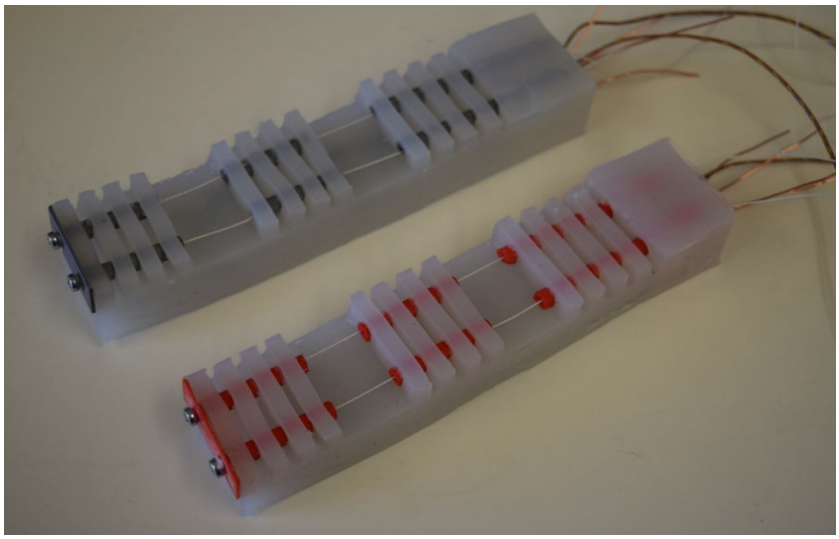

Figure 3.1: Two different kinds of fingers

3.1 Molds Design

To cast each layer of Field's metal, Ni-Cr heater, and tendon routed and also to pour the silicone compound, the molds are necessary and need to be fabricated with the same dimension to get the same size of layers.

3.1.1 Silicone Mold

In the case of the silicone mold, four acrylic walls with $6.35mm$ thickness and $45mm$ height were designed and fabricated as shown in Figure 3.2. They can be combined and fixed firmly with the clips to fit the finger's size. This method is convenient in detaching the cured silicone and flexible to control the size of a finger.

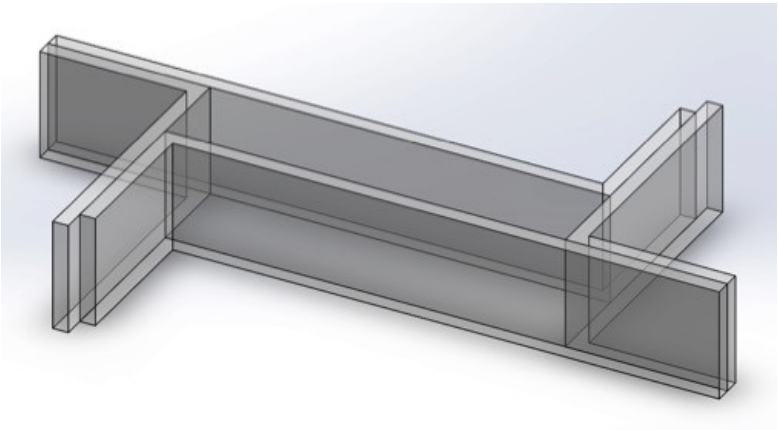

Figure 3.2: The silicone compound mold

3.1.2 Ni-Cr Wire Mold

Using Ni-Cr wire can be a great method in delivering the heat as quickly as possible. In the sense, the Ni-Cr wire needs to be wound to deliver the heat over the entire length of the metal rods while minimizing the added bending moment of the completed device. Also, it must be flattened as much as possible to deliver the heat evenly to the Field's metal rods. The molds were designed to combine and separate with two parts as seen in Figure 3.3 and the wires shaped such a way will be fixed with the silicone compound.

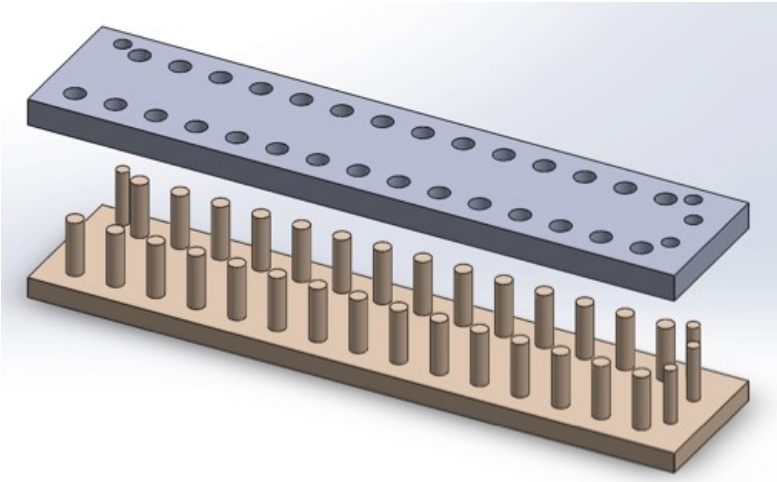

Figure 3.3: Ni-Cr wire casting mold

3.1.3 Field's Metal Mold

Structurally, two Field's metal rods are laid on the Ni-Cr layer to be heated. To grab both metal rods keeping the same distance, they need to become one layer inside the silicone compound. Also, the Field's metal rods need to be cast with the same dimension to support the whole device evenly. As seen in Figure 3.4, an injection mold with two cavities was fabricated by pouring the silicone compound in the acrylic mold. With this injection mold, the Field's metal rods can be manufactured flowing the molten metal solution through the broad opening.

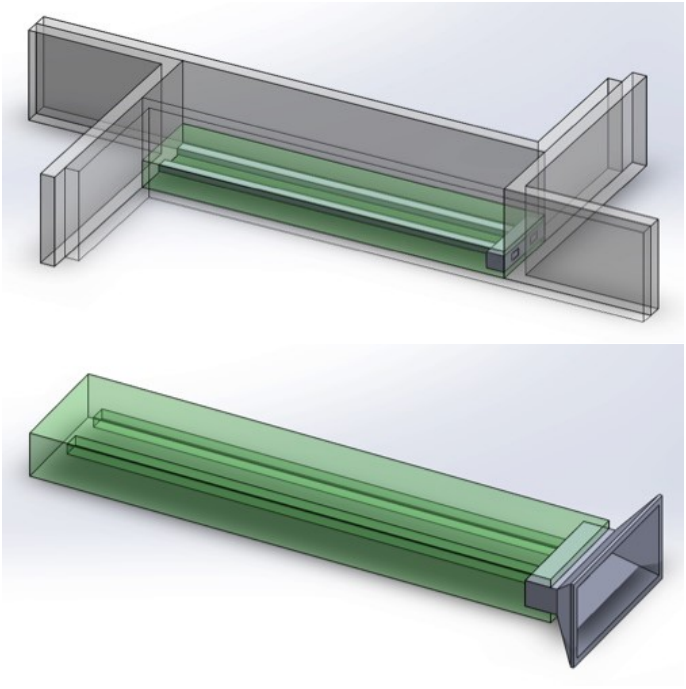

Figure 3.4: Field's metal casting mold

3.1.4 Top Surface Mold

The top surface of the finger has teeth to penetrate the thread through the holes in them and the tendon is pulled to drive the finger as a tendon. For casting this form of the surface, the mold for the top surface and the penetrating thread were designed and fabricated as seen in Figure 3.5. Two large teeth areas in the middle are positioned on the joints and to give free space while bending the finger. The holes through all teeth are to insert the sheath that the thread is supposed to penetrate them later. Except for the mold for pouring and solidifying the silicone compound, which was fabricated with the acrylics, all other molds to create Ni-Cr wiring, Field's metal rods, and teeth shape to rout tendons were fabricated by a 3d printer with ABS material.

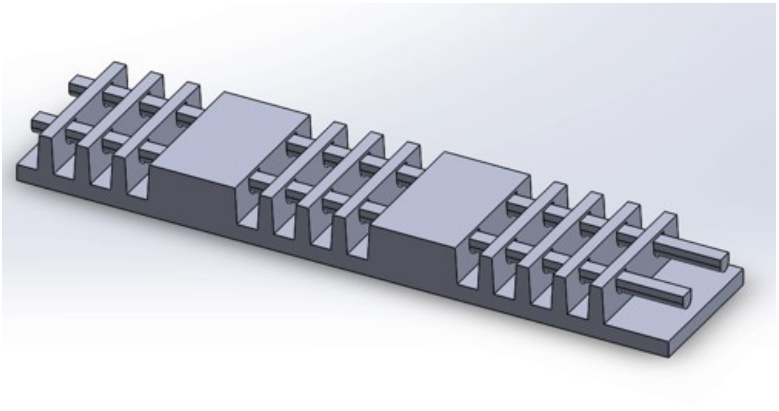

Figure 3.5: Surface mold for tendon-driven

3.2 Layer Fabrication

With the molds in the previous section, the fabrication process of each layer needs to be described. This section is explaining the detail procedure of how each material can be manufactured and layered using each mold.

3.2.1 Silicone Compound

The use of soft and deformable materials helps in the distribution of forces over a large contact area eliminating stress concentration within a soft robotic device [23]. In a sense of that, the silicone rubber can be considered as the primary material which is useful and necessary for fabricating the flexible robotic device. In here, two different silicone products were used. For a sample A, "Dragon Skin 10 Fast (Smooth-on Inc.)" was used and for another sample B, "Ecoflex 00-50 (Smooth-on Inc.)" was used. In order to de-gassed the uncured silicone compound, it should be in a vacuum chamber prior to pouring into the mold.

Item	Sample A	Sample B	Spec.
Elastomer	Dragon Skin 10 Fast	Ecoflex 00-50	
Mixed Viscosity	23,000 cps	8,000 cps	$ASTMD-2393$
Pot Life	8 min.	18 min.	$ASTMD-2471$
Cure Time	75 min.	3 hours	$None$
Shore A Hardness	10A	00-50	$ASTMD-2240$
Tensile Strength	475 psi	315 psi	$ASTMD-412$
100% Modulus	22 psi	12 psi	$ASTMD-412$

Table 3.1: Comparison between two silicone compounds

3.2.2 Ni-Cr Wiring Layer Casting

The 26 AWG Ni-Cr wire (diameter of $0.4039mm$ and $8.4354ohms/meter$) was used to fabricate it. First, a $1m$ length of wire was prepared. Using two molds in Figure 3.3, Ni-Cr wire was shaped along the protrusions. Then, the Ni-Cr wiring pattern is encased in the acrylic walls to pour the silicone compound. When the silicone compound is cured, the Ni-Cr wiring can be attached planar on the silicone surface as seen in Figure 3.6. The layers need to be fabricated as thin as possible not to make the whole thickness of the finger device being grown when each layer is

accumulated. The holes formed by protrusions on the mold can be refilled with the silicone compound during the fabrication process.

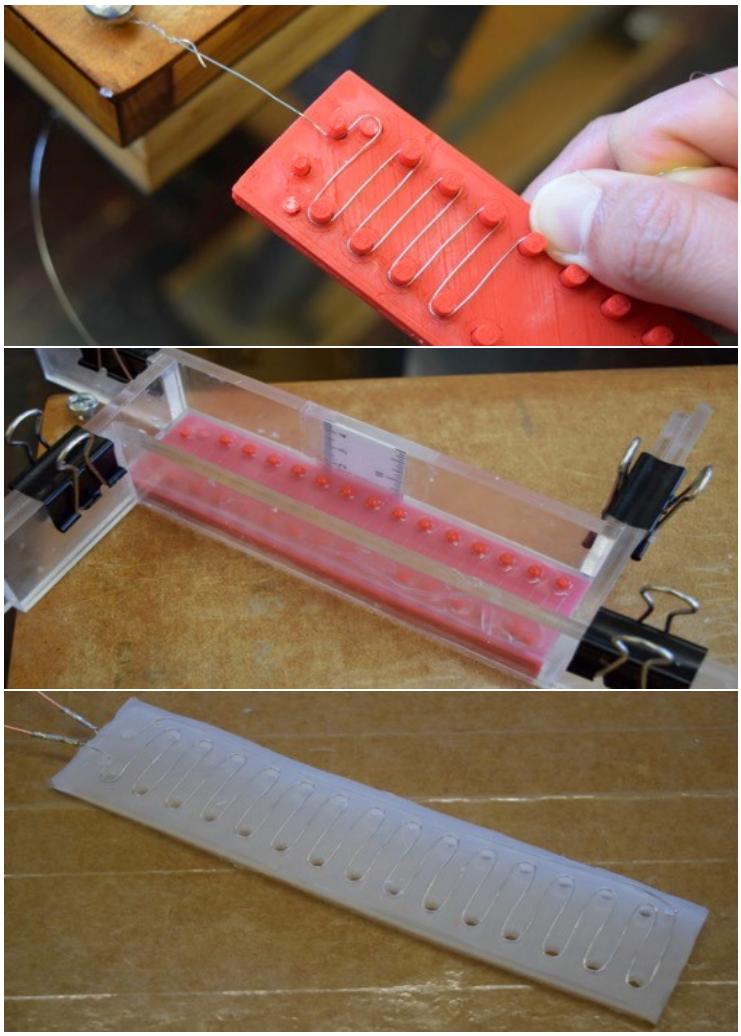

Figure 3.6: Ni-Cr wiring layer casting process

3.2.3 Field's Metal Rods Casting

For casting Field's metal rods, the silicone mold with cavities fabricated in advance as seen in Figure 3.4 was used. After inserting the injection device with the broad opening to the entrance of the silicone mold, the molten Field's metal solution is poured and let flow into the channels. When the Field's metal fluid is cooled and solidified, they are pulled out of the mold as seen in Figure 3.7. The dimension of a metal rod is $5 \times 3 \times 147.6mm$, and they will be laid on the Ni-Cr layer and cured by the silicone compound.

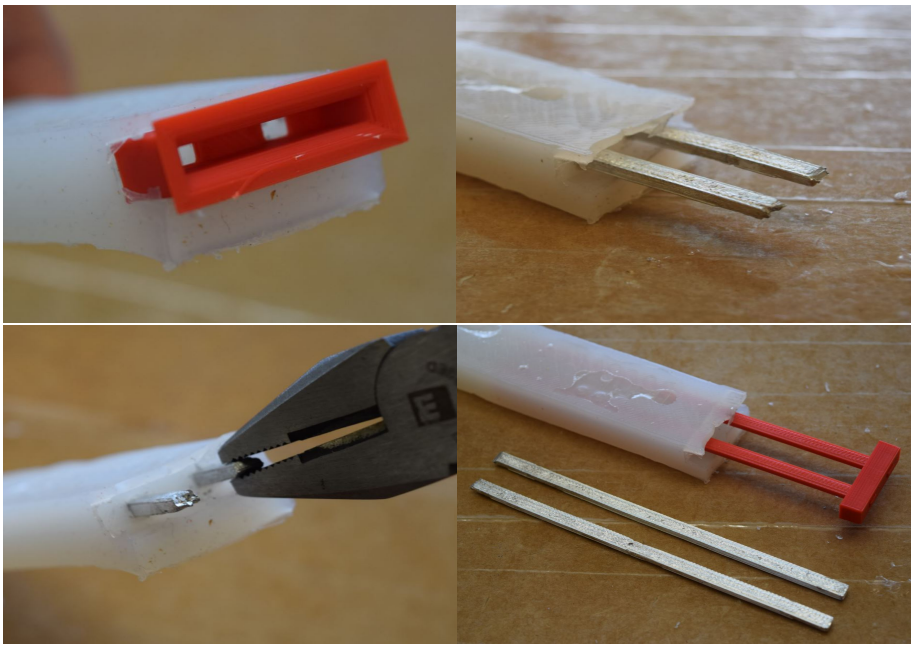

Figure 3.7: Field's metal rods casting process

3.2.4 Top Surface Layer

As seen in Figure 3.8, the top surface of finger device is fabricated using the mold designed in Figure 3.5. It is encased with the acrylic walls to fit the size, and the silicone compound is poured into it. After several hours, the silicone layer for the top surface with teeth comes out of the mold. The holes passing through the teeth is supposed to insert the sheath, and the thread can pass through the sheath to be a role of the tendon.

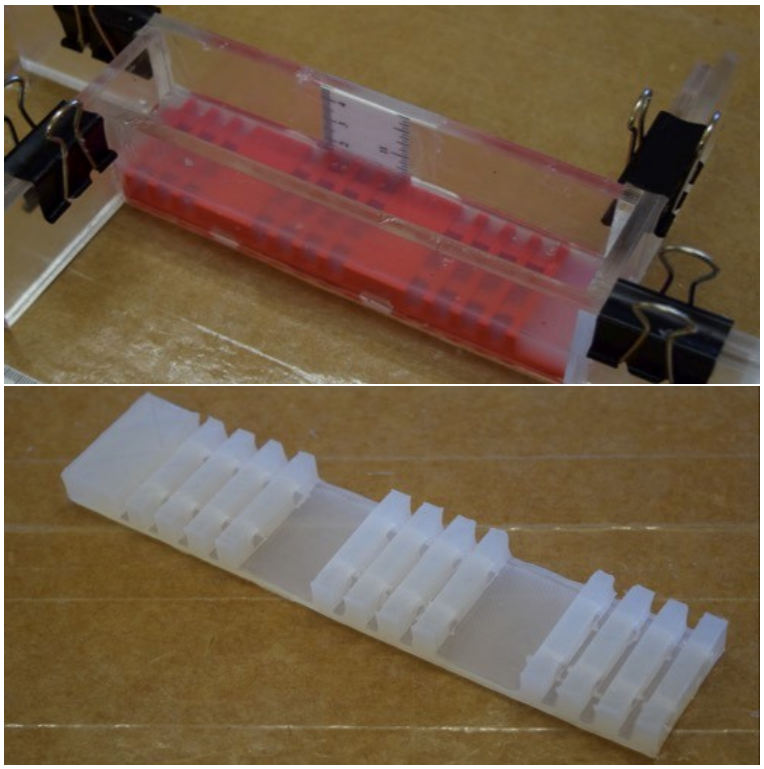

Figure 3.8: Top surface layer casting process

3.3 Finger Manufacturing Process

With each layer of Ni-Cr wiring, Field's metal rods, and tendon routed fabricated using each mold, sample A, and B were built through the following process. Sample A has three layers and sample B has four layers as seen in Figure 3.9-(Bottom).

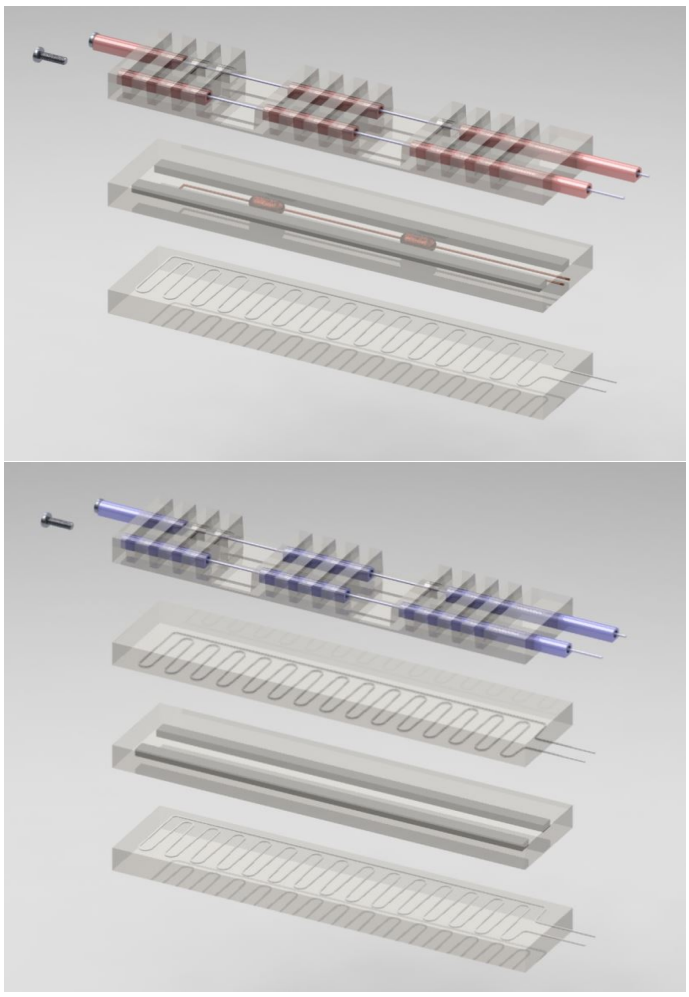

Figure 3.9: Layer by layer process of sample A (top) and B (bottom)

3.3.1 Sample A

In the case of sample A, the silicone compound with high viscosity and quick cure time was used (Dragon Skin 10 Fast). The heating elements were used with one down layer of Ni-Cr wiring plus the power resistors. The concept of this sample is that one Ni-Cr wiring layer raises up the temperature close to 50-55 °C and the rest of temperature to the melting point of Field's metal is supposed to be done by the power resistors positioned in the finger joints.

At first, the Ni-Cr layer with holes by projections for winding the wire is encased in the acrylic walls as the first layer. A little amount of silicone compound is poured and spreads out evenly to fill out the holes. Two power resistors (each $5.6 ohms$, $5 watts$) are prepared with a serial connection and positioned in the middle of two Field's metal rods. Also, two thermocouple glass braids are embedded to measure the temperature of each Ni-Cr wire and power resistor. Another little amount of silicone is poured and spread out evenly to be approximately 1-2mm height. The top surface layer is placed on it to become complete finger device as shown in the last picture down below of Figure 3.10. After cured the silicone compound completely, the acrylic molds are disassembled, and sample A becomes completed finally.

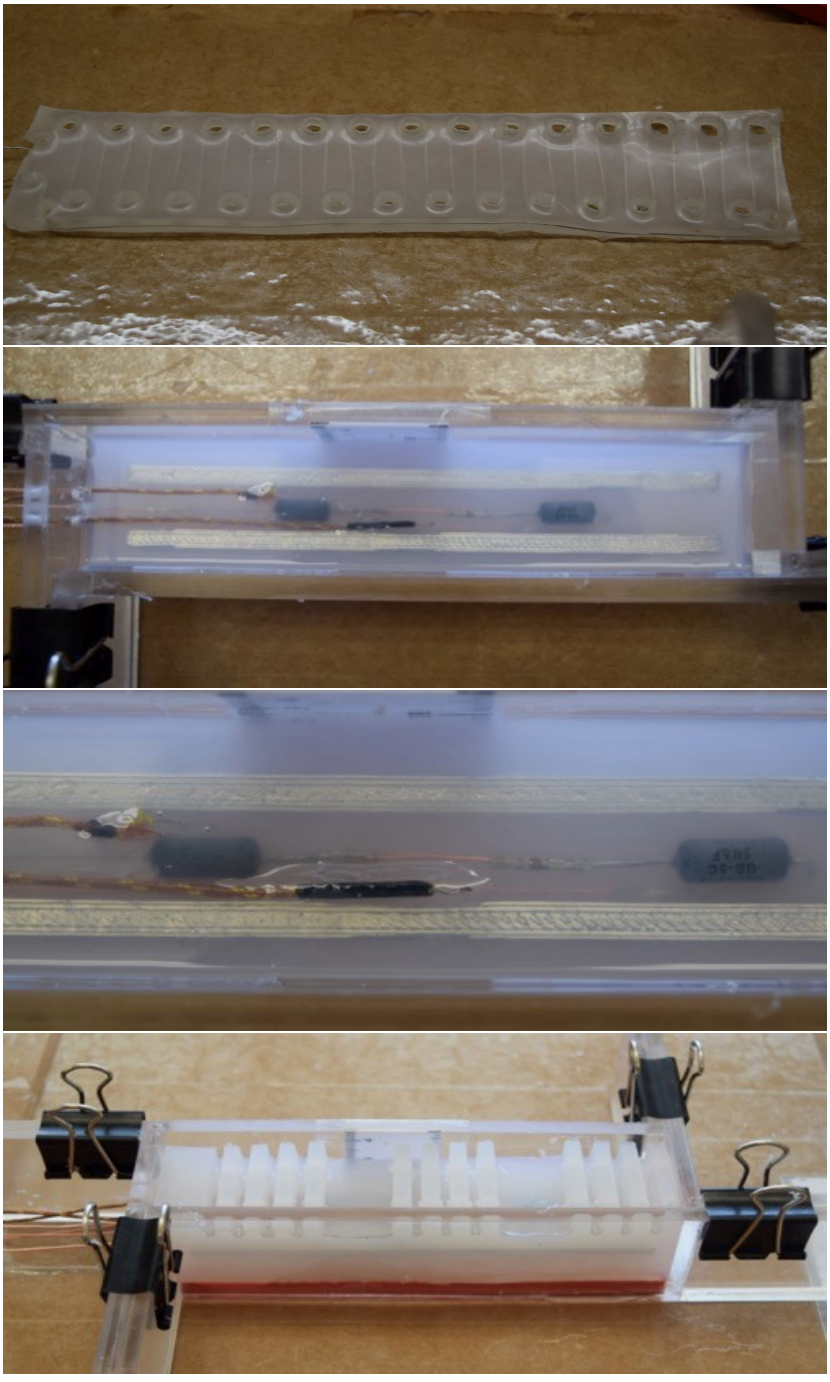

Figure 3.10: Fabrication process of sample A

3.3.2 Sample B

Sample B used the silicone compound with less viscosity and strength was used (Ecoflex 00-50). Two Ni-Cr layers positioning above and below the metal layer were used as heaters to melt the Field's metal rods globally. One thermocouple glass braid was embedded to measure the temperature.

For manufacturing it, one Ni-Cr layer is placed in the acrylic mold, and a little amount of silicone compound is poured and spread out evenly to be 1-2mm height. Two Field's metal rods with approximately 10-11mm gap are laid on the Ni-Cr layer, and another amount of silicone compound is added to let the metal rods sink with 1-2mm height. After it is cured, the second Ni-Cr layer is placed on it and poured the little amount of silicone compound again. For the final step, the top surface layer is put on the second Ni-Cr layer and let them be cured with the silicone compound. When all layers are completely cured with the silicone compound, the silicone walls are detached to get sample B.

The sheaths for penetrating thread by the 3d printer are inserted into the holes on the top layer. One end of the thread is tied up to $M3 \times 6$ bolt, and it is fixed on the end of the sheath. The wire of thermocouple glass braids is also out of the body and the Ni-Cr wire connects to the bare copper wire.

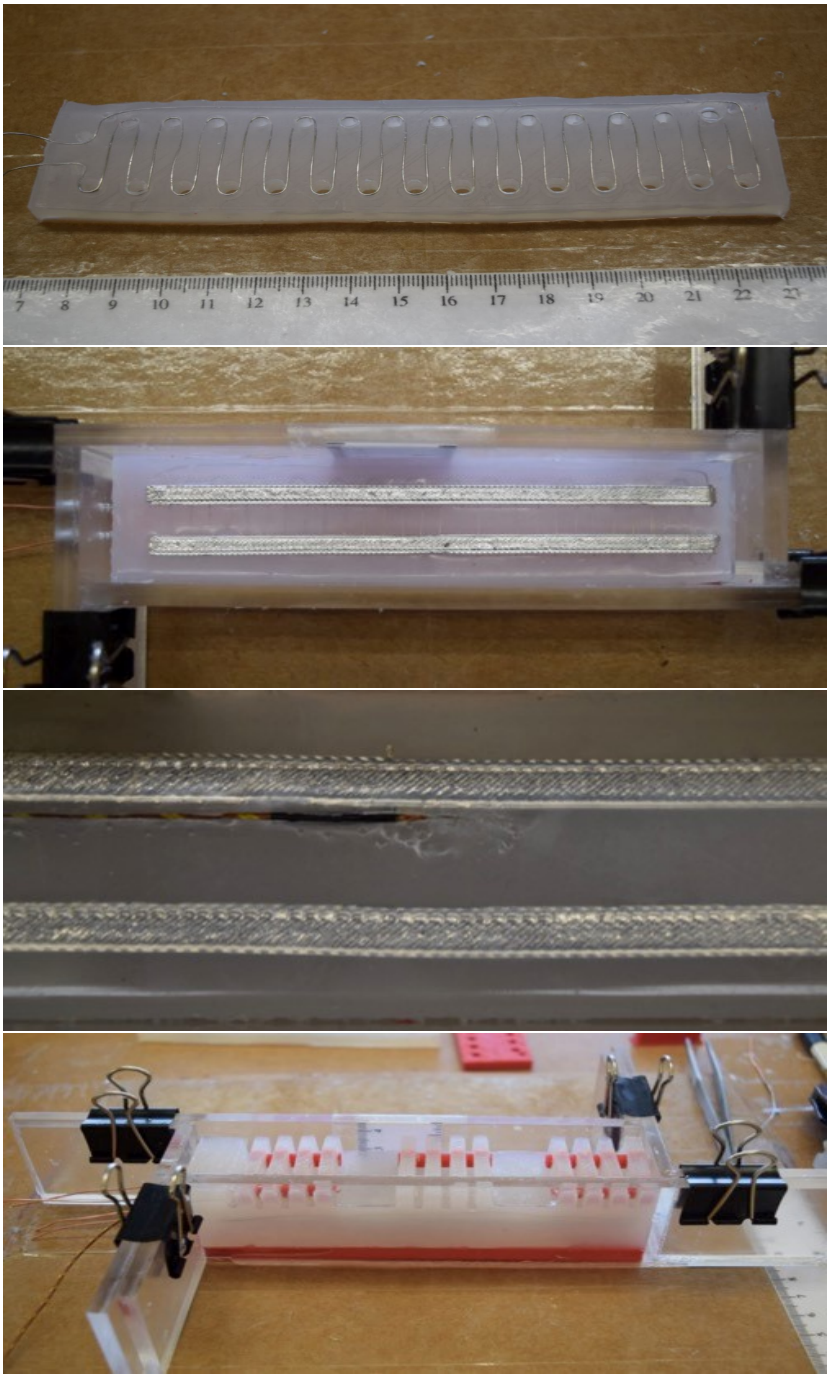

Figure 3.11: Fabrication process of sample B

Finally constructed finger devices have $35 \times 30 \times 172mm$ size as presented in Figure 3.12.

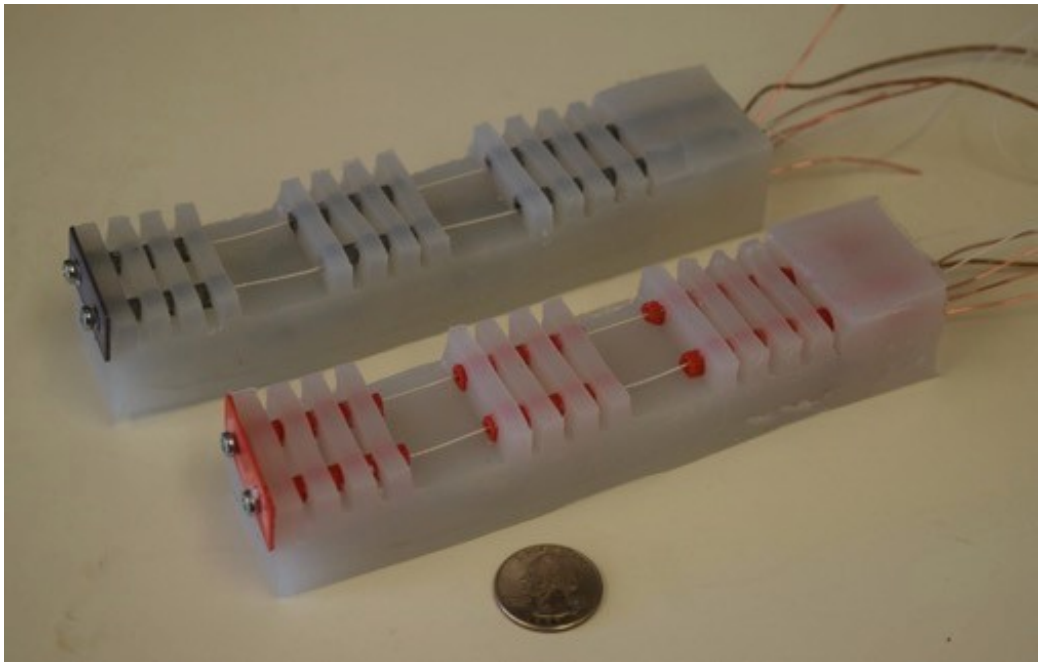

Figure 3.12: Completion of sample A (top) and B (bottom)

CHAPTER 4. EXPERIMENTS

In order to conduct experiments, the test setup was configured with a power supply device, thermocouple amplifiers, a Chipkit uC32 board, and a laptop to run the Arduino code to observe the temperature variation on every second as seen in Figure 4.1. The experiments are mainly to figure out the following points and conducted for each finger samples independently.

- The time required to reach the melting point (62 °C)
- The temperature fluctuation required from the biasing point to achieve localize or global melting
- The measured thermocouple temperature that corresponds to liquefaction and solidification of the metal
- Demonstration of local or global stiffness changes

First, it is supposed to measure how long the device takes to bias the temperature up to the melting point, 62 °C. Secondly, it is to measure how fast the temperature goes above and below the melting point. This experiment allows us to understand that the rate at which the device can vary from its stiff to compliant regimes and vice versa. Third, it is to figure out accurate temperature to melt down

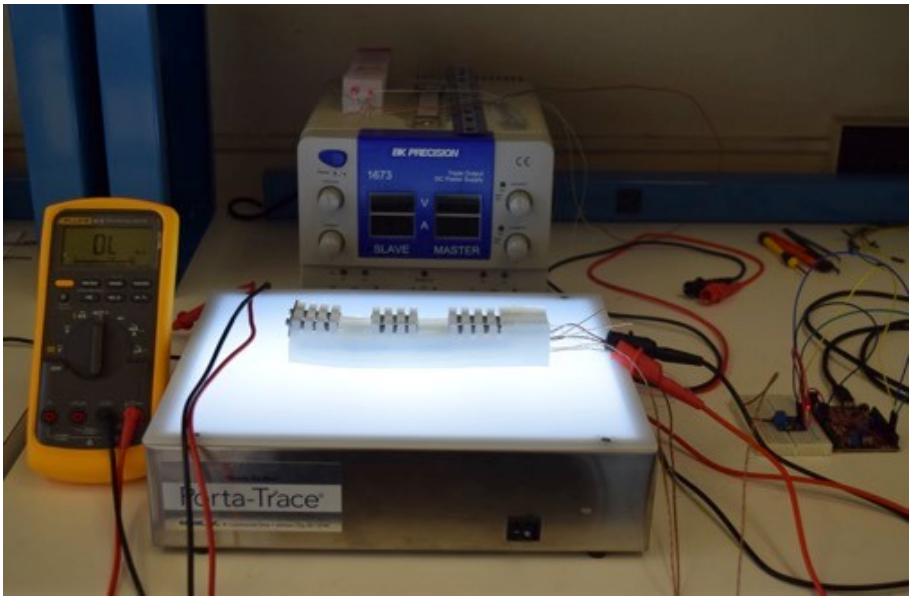

Figure 4.1: Test set-up with a multimeter, power supply, and Chipkit uC32 board

the rods completely which mean liquefied. The metal rods are embedded in the silicone compound, therefore, the temperature to melt them down would be higher than the theoretical melting point 62 °C due to indirect contact to the heating element. Lastly, it is observed from various perspectives when the finger device is bending.

The Ni-Cr wiring was used approximately 1-1.1m length. The resistance per length of the Ni-Cr 26AWG is 8.4354$ohm/meter$, and the total resistance of each wire was measured with 8.6ohm taking into account the resistance of the connectors and bare copper wires. The resistance of power resistor is 5.6ohm, and it was measured with 11.4ohm for two resistors in serial connection with connectors and bare copper

wires. The maximum power capacity of each resistor is $5watt$. The thermocouple glass braid wire's ends were connected to the thermocouple amplifier, which in turn was analog to digital converter of the Chipkit uC32 board. While running the Arduino codes for temperature measurement, the power supply was regulated with the voltage and current. The room temperature was approximately 24 °C, and the measurement started as soon as power supply was switched on.

4.1 Rate of Change of Temperature from 24 °C to 62 °C

The purpose of this experiment is to figure out how fast the temperature can reach the actual melting point, 62 °C and how the rate of temperature change will be presented.

4.1.1 Sample A

Sample A was planted with two thermocouple glass braids as seen in Figure 3.8 and it was measured for each point with different power supply. At first, both heating elements were supplied with maximum electric power and then Ni-Cr wire was powered only. When dual heaters were used, the starting temperature was 27.5 °C and for the single heater, it was started from 28 °C and reached 28.5 °C after the $50s$.

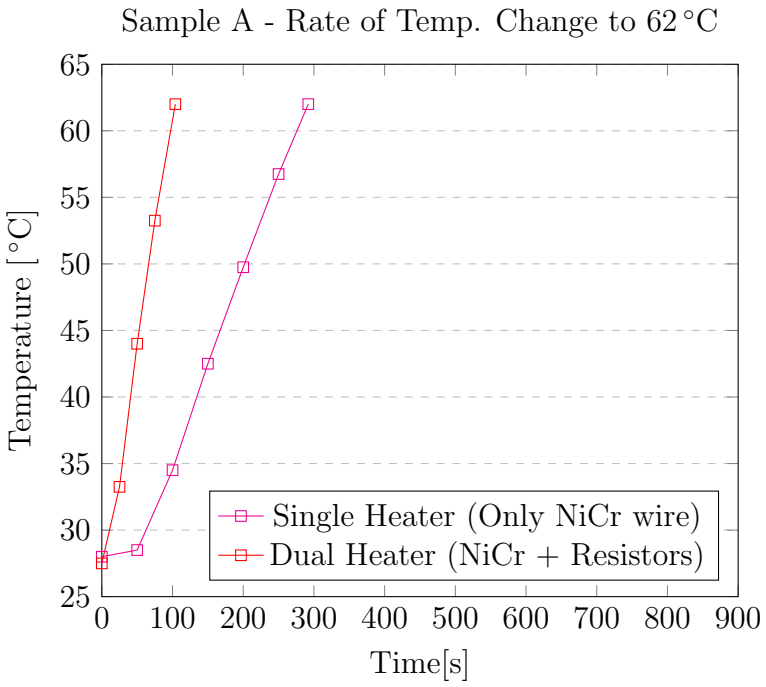

4.1.2 Sample B

In the case of sample B, only one thermocouple glass braid was implanted because it has one kind of heating elements layered up and down to deliver the heat globally. The first measurement was done with the electric power $8.4watt(1.0A, 8.4V)$ for each Ni-Cr wire and the second one done with reduced power to $4.2watt$.

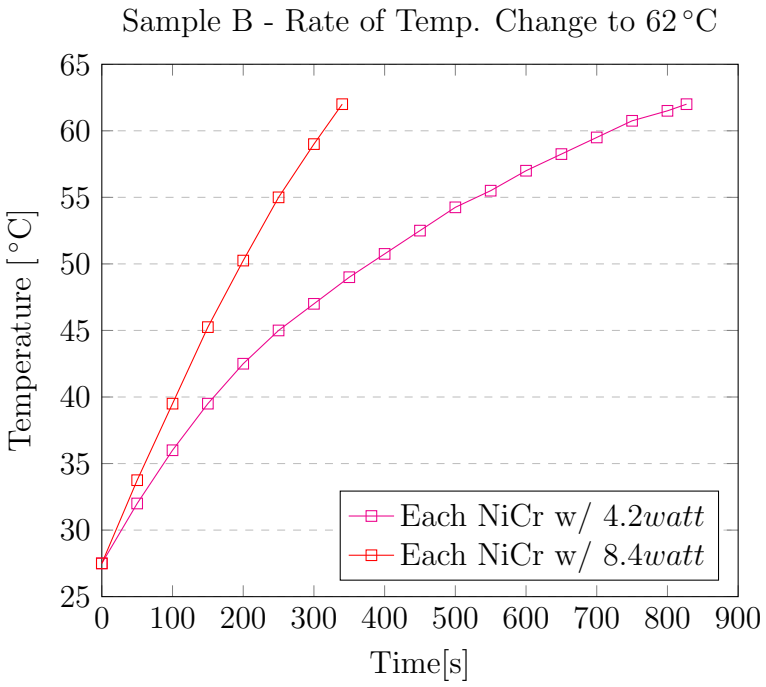

4.2 Fluctuation of Temperature between 50 °C and 70 °C

Assuming the temperature area for liquefying and solidifying the metal with 50 °C and 70 °C respectively, the experiment was conducted to figure out how fast the rate of change of temperature can fluctuate. The power was on and off repetitively for increasing and decreasing the temperature within the range.

4.2.1 *Sample A*

For sample A, it was measured at only the point where the thermocouple glass braid is planted near both Ni-Cr wire and resistor because it is considered as a joint area of finger device.

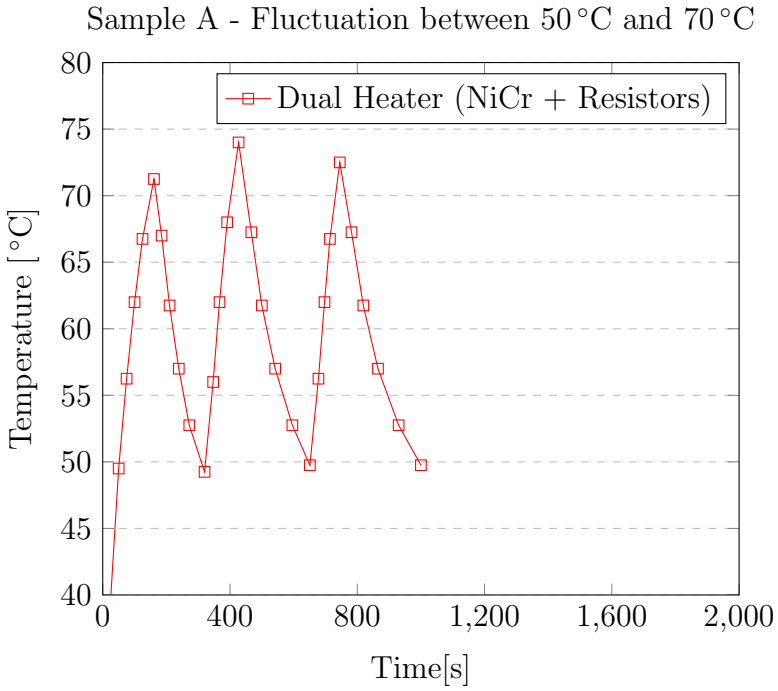

4.2.2 *Sample B*

As seen in below plot, it was measured two cycles under the electric power 8.4*watt* for each Ni-Cr wire layered above and below the metal rods.

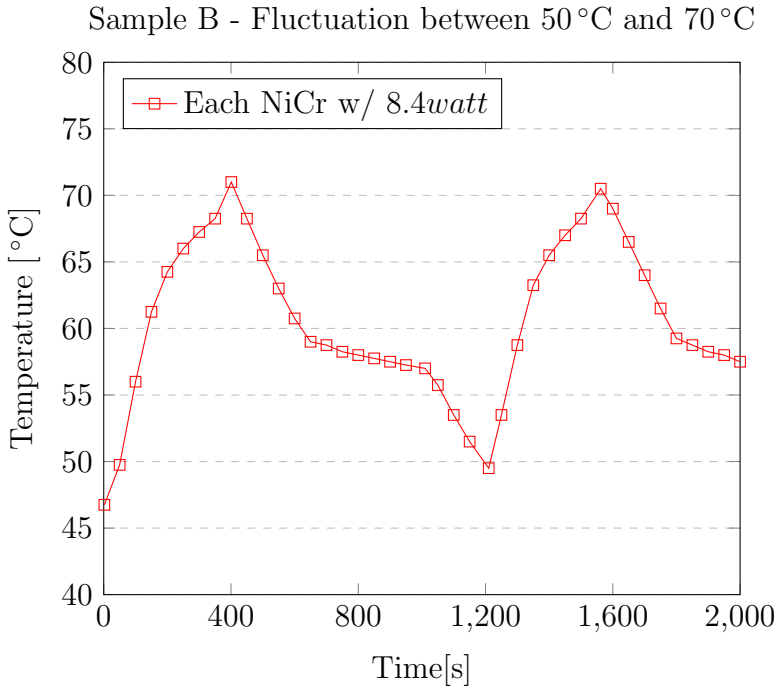

4.3 The Temperature of Liquefying and Solidifying the Metal

In order to find the actual temperature area to liquefy and solidify the metal rods, this experiment was conducted. While monitoring the temperature, the finger kept bending continuously with the maximum power of heaters. The cooling process was on the same way.

4.3.1 Sample A

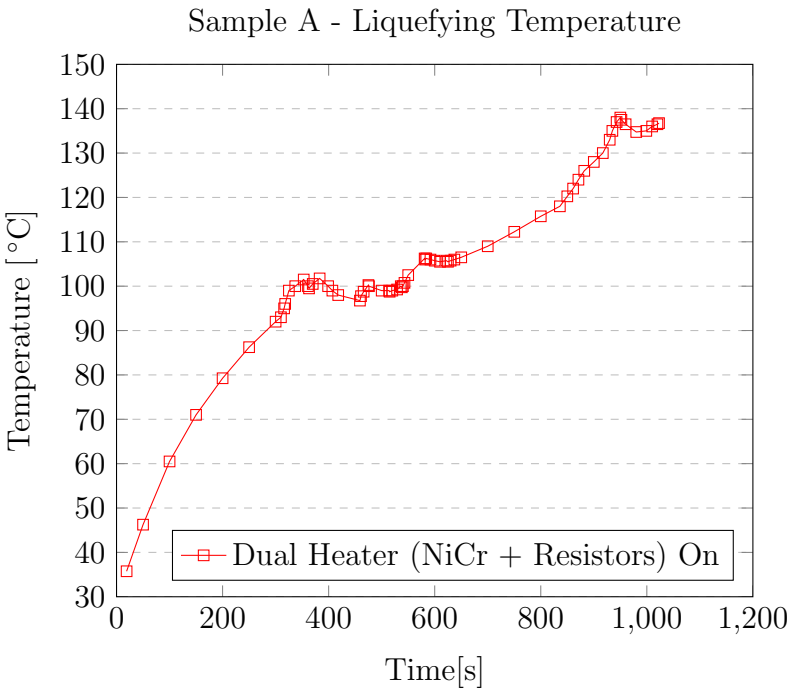
Sample A - Liquefying Temperature
Temperature [°C]
Time[s]
Dual Heater (NiCr + Resistors) On
150
140
130
120
110
100
90
80
70
60
50
40
30
0
200
400
600
800
1,000
1,200

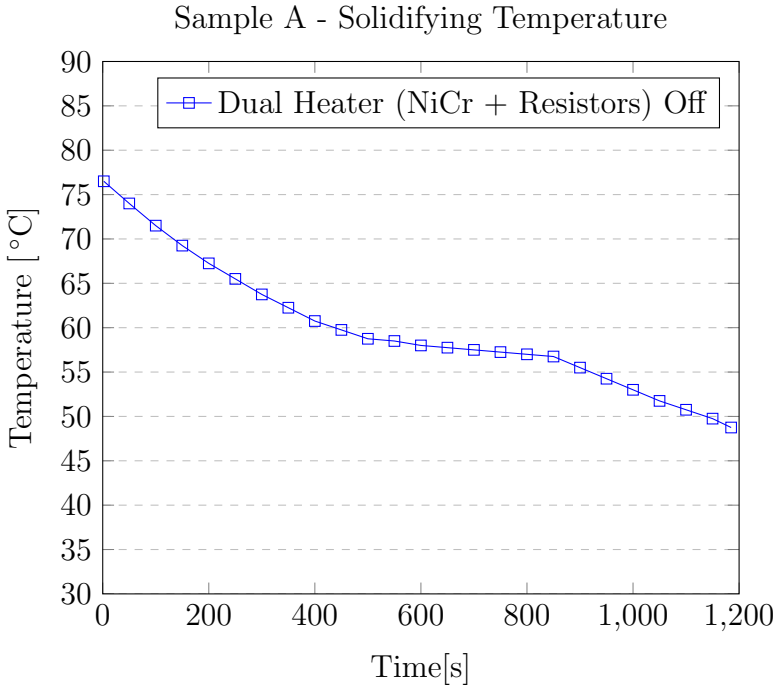
Sample A - Solidifying Temperature
Temperature [°C]
Time[s]
Dual Heater (NiCr + Resistors) Off
90
85
80
75
70
65
60
55
50
45
40
35
30
0
200
400
600
800
1,000
1,200

4.3.2 Sample B

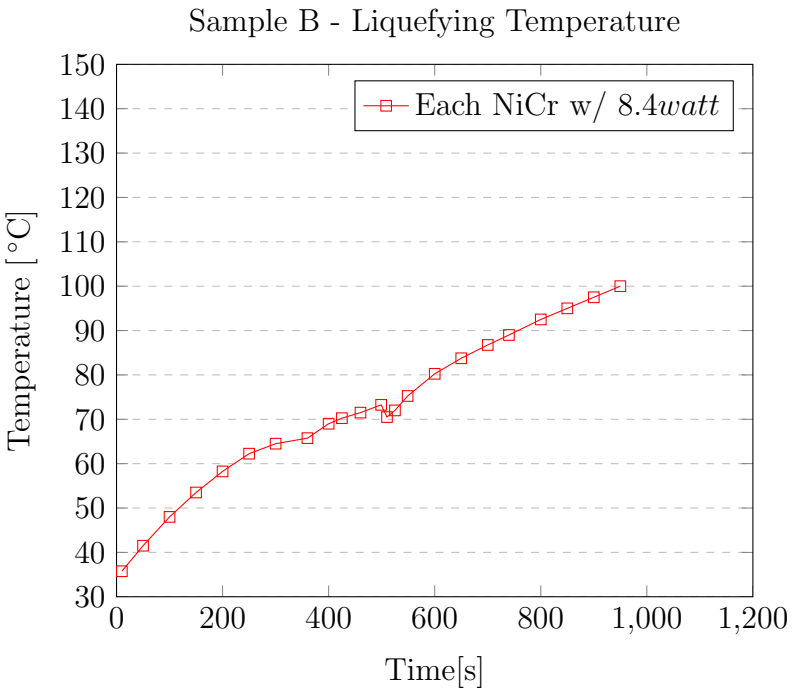
Sample B - Liquefying Temperature
Each NiCr w/ 8.4watt
Temperature [°C]
Time[s]
150
140
130
120
110
100
90
80
70
60
50
40
30
0
200
400
600
800
1,000
1,200

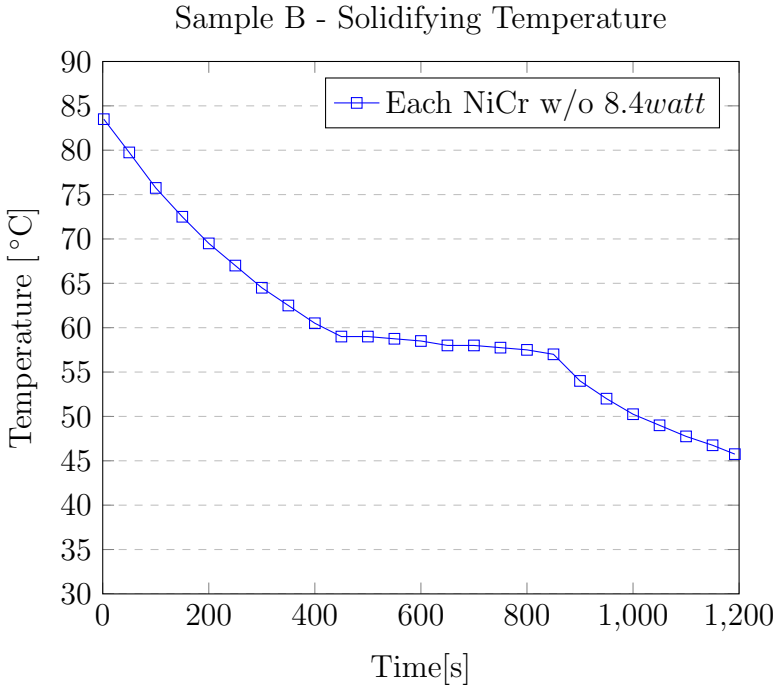
Sample B - Solidifying Temperature
Each NiCr w/o 8.4watt
Temperature [°C]
Time[s]
90
85
80
75
70
65
60
55
50
45
40
35
30
0
200
400
600
800
1,000
1,200

4.4 Device Actuation and Kinematics

The final aspect of the tunably-compliant fingers is the ability to control both the melting of the skeleton, either at specific locations within the device or globally and to cause bending using the tendon routed through the device. In sample A, shown in Figure 4.2-(Top), the bending is concentrated at the spatial location where the power resistors have caused localized melting of the Field's metal skeleton. In contrast, sample B, shown in Figure 4.2-(Bottom), the bending is continuous across the entire device as the heating has caused global melting of the Field's metal skeleton. Another difference between the two samples was the required force for deformation. Because sample B was fabricated with the less stiff Ecoflex 00-50 silicone rubber, the tendon forces required to deform the finger were less than the forces required for sample A.

From the standpoint of the kinematics of the devices, sample B could be described using standard models for large-deflection of highly elastic beams. On the other hand, devices like sample A where the bending is concentrated in small regions of the total device, simplified models of compliant mechanism as pin joints with torsional springs can be applied [24].

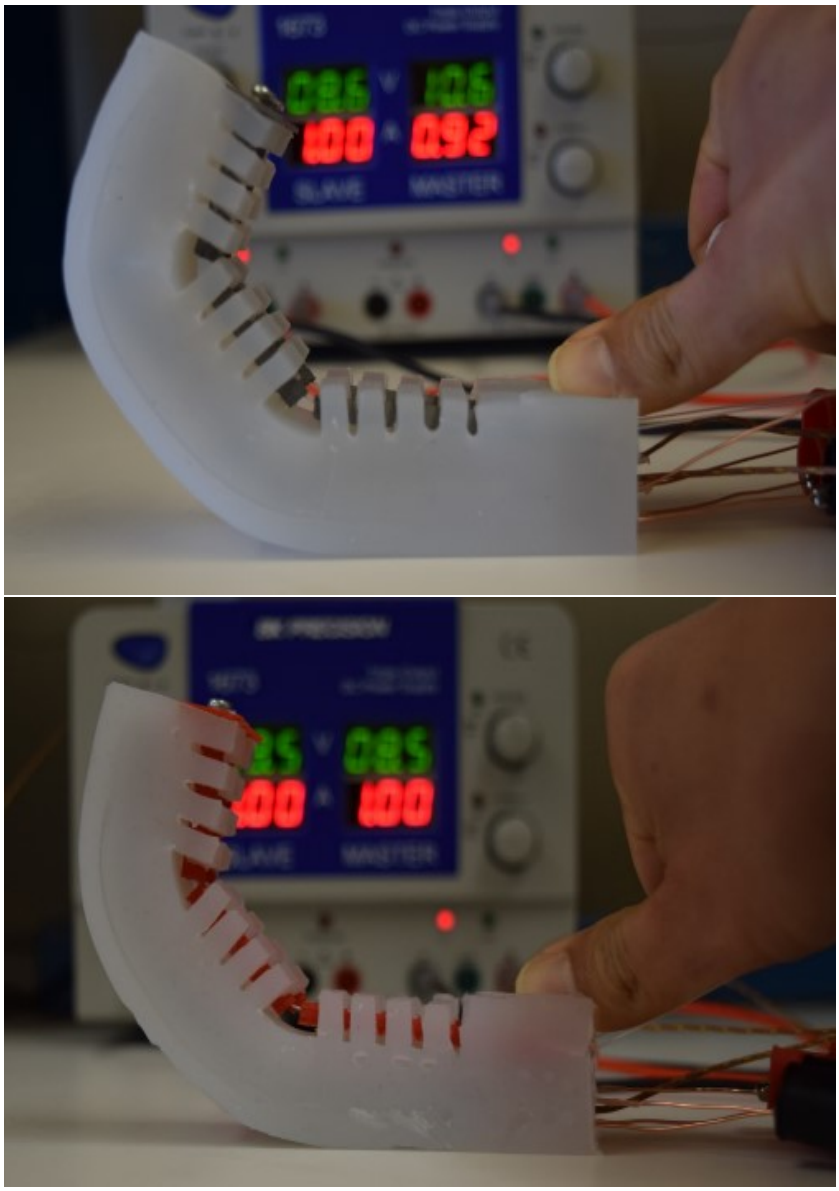

Figure 4.2: Segmented bending with localized heating of sample A (Top). Continuous bending with global heating of sample B (Bottom)

CHAPTER 5. THERMAL ANALYSIS AND SIMULATION

Apart from the direct measurement by the experiments with samples, it is important to use the thermal analysis and simulation because it can predict the temperature in advance before the sample is designed and manufactured. This chapter presents the thermal analysis of the device with some equations in thermodynamics and applied them into the sample A. Also, thermal simulation by the program, Solidworks (Dassault Systems, Waltham, Massachusetts, USA) is done for the transient thermal behavior of using each material's thermal properties. Before the simulation by the program, the theoretical thermal calculation was done first. The steady state behavior of the materials was calculated using the thermal mechanism by which heat is transferred such as conduction and convection. In here, only thermal resistance by conduction and convection was considered. The thermal resistance R for heat transfer is defined as the ratio of the change in temperature difference to the change in heat flow rate [25].

$$R = \frac{dT}{dq_h} \tag{5.1}$$

The thermal resistance R has units of $K{\cdot}s/J$, $^{\circ}\mathrm{C}{\cdot}s/J$, or $^{\circ}\mathrm{F}{\cdot}s/(ft{\cdot}lb)$. For simple one-dimensional conduction can be given by the law of heat conduction

$$q_h = kA\frac{\Delta T}{L} = kA\frac{T_1 - T_2}{L} \tag{5.2}$$

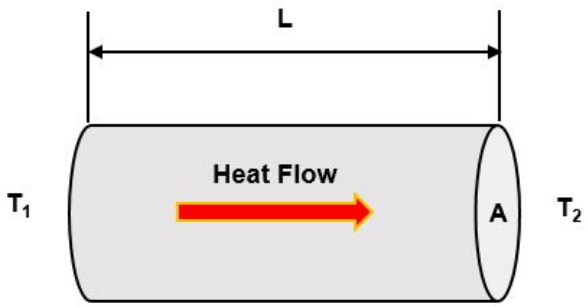

Figure 5.1: One-dimensional conduction heat flow

In Figure 5.1, L is the length of the body, A is the cross-sectional area normal to the heat flow direction, ΔT is the temperature difference along the length, and k is the thermal conductivity of the material in $W/(m{\cdot}K)$ or $W/(m{\cdot}\,^{\circ}\mathrm{C})$. Combining 5.1 and 5.2 can give the thermal resistance for conduction like below [25].

$$R = \frac{L}{kA} \tag{5.3}$$

For convective heat transfer, the rate of heat flow of the body is proportional to the difference in temperature between the body and its environment. Therefore, the mathematical expression can be given as

$$q_h = hA\Delta T = hA(T_{sur} - T_{env}) \tag{5.4}$$

where A is the surface area, from which the heat is transferred, T_{sur} is the temperature of the body surface, T_{env} is the temperature of the environment, and h is the heat transfer coefficient in $W/(m^2 \cdot K)$ or $W/(m^2 \cdot {}^\circ\mathrm{C})$. Combining 5.1 and 5.4 can give the thermal resistance for convection like following.

$$R = \frac{1}{hA} \tag{5.5}$$

It is useful to utilize the concept of thermal resistance and represent heat transfer by a thermal circuit such that the heat flow rate q_h is analogous to the current, the temperature difference ΔT is considered as the voltage, and the thermal resistance can be the electric resistance. For the composite slab with the thermal resistance in series interconnection R_1 and R_2 can be resulted with $T_1 - T_2 = R_1 q_h$ and $T_2 - T_3 = R_2 q_h$ respectively. The total temperature difference across the composite slab is $T_1 - T_3 = (R_1 + R_2)q_h$. Thus, the equivalent thermal resistance for a series interconnection is like following [25].

$$R_{eq} = R_1 + R_2 \tag{5.6}$$

Item	Thermal Conductivity	Specific Heat	Mass Density
Unit	$W/(m \cdot K)$	$J/(kg \cdot K)$	kg/m^3
Field's Metal	18.5	285	7888.77
NiCr wire	11.3	450	8400
Hot End Resistor	1.5	877.96	2300
Silicone Rubber	1.2	1175	1700

Table 5.1: Each material's properties

5.1 Thermal Analysis of the Steady State Behavior

With above concept, using the section view of sample A as shown in Figure 5.2, the little size of red squares can be considered and also calculated with the cross-sectional area of each wall and the thickness of each wall. Therefore, it can be represented using a thermal circuit with five thermal resistances connected in series as shown in Figure 5.3. First, each cross-sectional area is calculated with the length of the hot end resistor $7.2mm$ and the same length of the square $3mm$. Therefore, the cross-sectional area is that $0.0072m \times 0.003m = 2.16 \times 10^{-5}m^2$. The thermal properties of each material are shown in table 5.1. Therefore, the calculation of each wall's thermal resistance can be calculated like below.

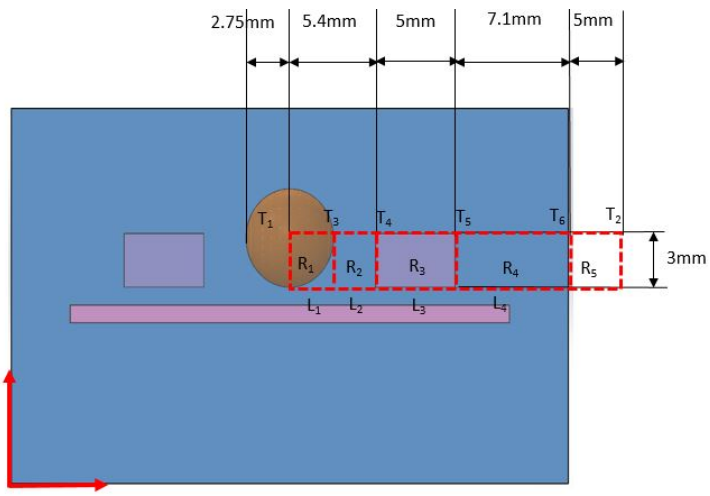

Figure 5.2: Section view of sample A

- $R_1 = L_1/(k_1 \times A) = 0.00275/(1.5 \times 2.16 \times 10^{-5}) = 848.765Ks/J$
- $R_2 = L_2/(k_2 \times A) = 0.00265/(1.2 \times 2.16 \times 10^{-5}) = 1022.377Ks/J$
- $R_3 = L_3/(k_3 \times A) = 0.005/(18.5 \times 2.16 \times 10^{-5}) = 125.125Ks/J$
- $R_4 = L_4/(k_4 \times A) = 0.0071/(1.2 \times 2.16 \times 10^{-5}) = 2739.198Ks/J$
- $R_5 = 1/(h_5 \times A) = 1/(2731.5 \times 2.16 \times 10^{-5}) = 169.490Ks/J$

From R_1 to R_4 is the heat transfer by the conduction with thermal conductivity of k_1, k_2, k_3, and k_4 and the last R_5 is the heat transfer by the convection of the air's convection coefficient $10W/m^2 \cdot^\circ$ C$(= 2731.5W/m^2 \cdot K)$. According to the equation 5.6, the total thermal resistance is

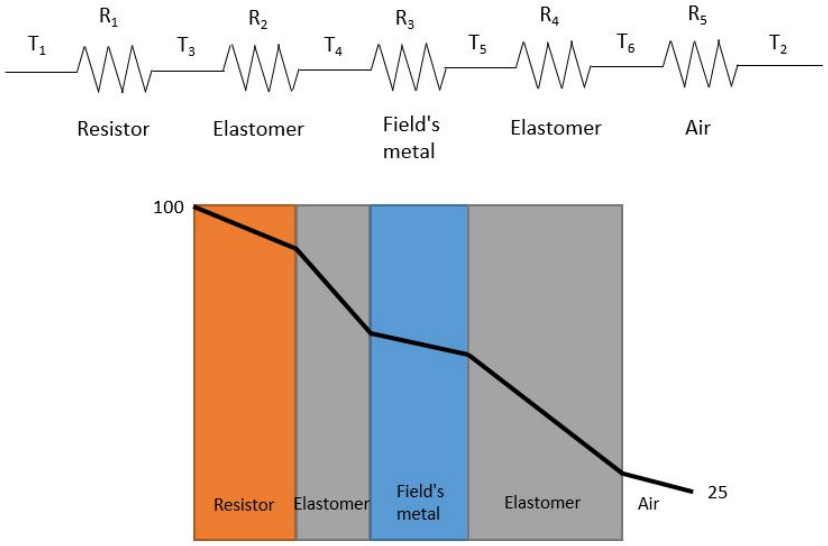

Figure 5.3: The thermal resistances circuit for the heat transfer

$$R_{eq} = \sum_{i=1}^{5} R_i = 4904.955 Ks/J$$

Thus, the heat flow rate from $T_1 = 100\,^{\circ}\text{C}$ to $T_2 = 25\,^{\circ}\text{C}$ through the insulated wall is

$$q_h = \frac{\Delta T}{R_{eq}} = \frac{(373.15K - 298.15K)}{4904.955 Ks/J} = 0.0153W$$

The heat flow rate stays the same through the insulated wall. Thus, from left to right, the heat flow rate through each layer is

$$Resister : q_h = \frac{(T_1 - T_3)}{R_1} \Rightarrow T_3 = 360.17K(87.0\,^\circ\mathrm{C})$$
$$Elastomer : q_h = \frac{(T_3 - T_4)}{R_2} \Rightarrow T_4 = 344.54K(71.4\,^\circ\mathrm{C})$$
$$Metal : q_h = \frac{(T_4 - T_5)}{R_3} \Rightarrow T_5 = 342.63K(69.5\,^\circ\mathrm{C})$$
$$Elastomer : q_h = \frac{(T_5 - T_6)}{R_4} \Rightarrow T_6 = 300.74K(27.6\,^\circ\mathrm{C})$$
$$Air : q_h = \frac{(T_6 - T_2)}{R_5} \Rightarrow T_2 = 298.15K(25.0\,^\circ\mathrm{C})$$

From the above, the temperature from the initial heat source is reduced by each material's thermal resistance such as $T_1 = 100\,^\circ\mathrm{C} \rightarrow T_3 = 87.0\,^\circ\mathrm{C} \rightarrow T_4 = 71.4\,^\circ\mathrm{C} \rightarrow T_5 = 69.5\,^\circ\mathrm{C} \rightarrow T_6 = 27.6\,^\circ\mathrm{C} \rightarrow T_2 = 25\,^\circ\mathrm{C}$.

In order to figure out the temperature tendency in the device over time, the thermal flow should be analyzed based on the first law of thermodynamics. For a system with well-defined boundaries, the law of energy conservation states

$$\Delta E = Q - W \tag{5.7}$$

ΔE is the change in energy of the system, Q is the heat flow into or out of the system, and W is the work done by or on the system [25]. In actuality, the net amount of

energy added to the system is equal to the net increase in the energy stored internally in the system and any change in the mechanical energy of the system's center of mass,

$$\Delta E = \Delta U + \Delta ME_C \tag{5.8}$$

U is the internal thermal energy stored at the molecular level and ME_C stands for the mechanical energy including the kinetic and the potential energy associated with the system's mass center. For the systems with negligible change in mechanical energy,

$$\Delta U = Q - W = (Q_{in} - Q_{out}) - (W_{out} - W_{in}) \tag{5.9}$$

which is the mathematical expression of the first law of thermodynamics. For thermal systems with pure heat transfer and no work involved, that is $W_{in} = W_{out} = 0$, the law of energy conservation can be presented as

$$\Delta U = Q = Q_{in} - Q_{out} \tag{5.10}$$

or

$$\frac{dU}{dt} = q_{hi} - q_{ho} \tag{5.11}$$

where $q_h = dQ/dt$ is the heat flow rate having units of J/s, which is a $watt$ or $ft{\cdot}lb/s$ [25].

There is another important concept of the thermal calculation. It is the thermal capacitance C which is the measure of the heat required to increase the temperature of the object by a certain temperature interval. It is defined as the ratio of the change in heat flow to the change in the object's temperature.

$$C = \frac{dQ}{dT} \tag{5.12}$$

where C has units of J/K, $J/^{\circ}$C, or $ft \cdot lb/^{\circ}$F. For a constant-volume process, if it is assumed that no work is involved and all the heat goes into the internal energy of the substance,

$$Q = \Delta U = mc_v \Delta T \tag{5.13}$$

m is the mass of the substance, c_v is the constant-volume specific heat capacity of the substance in units of $J \cdot K/kg$, $J \cdot^{\circ}$ C$/kg$, or $ft \cdot lb^{\circ} \cdot$ F$/slug$, and ΔT is the change in temperature of the substance. Combining Equation 5.12 with Equation 5.13 and assuming that the density and the volume of the mass are ρ and V, respectively, it is given such as,

$$C = mc_v = mc = \rho V c \tag{5.14}$$

where c is the specific heat capacity depending on the substance of the object itself, whereas the thermal capacitance C can be proportional to the mass of the object [25].

5.2 Thermal Analysis of Transient Behavior

Using the Equation 5.11 and 5.14 above, the differential equation relating the temperature of very near the heater's surface T_1 and the temperature of very near the metal's surface T_2 can be derived as shown in figure 5.4.

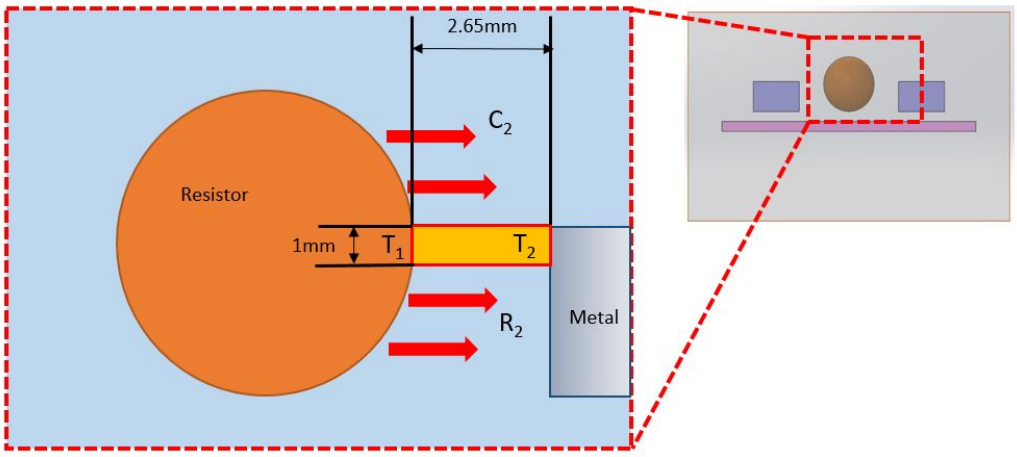

Figure 5.4: Temperature dynamics of a heated object

Applying the law of conservative of energy to the elastomer, it is

$$\frac{dU}{dt} = q_{hi} - q_{ho}$$

where $U = mcT_2 = \rho V c T_2$, and we have

$$\frac{dU}{dt} = \frac{d}{dt}(\rho V c T_2) = \rho V c \frac{dT_2}{dt}$$

The heat flow rate from the heater to the elastomer q_{hi} is represented like below and the heat flow rate on the opposite way (out of the elastomer) $q_{ho} = 0$.

$$q_{hi} = \frac{T_1 - T_2}{R_2}$$

where R_2 is the thermal resistance of the elastomer. Thus, the differential equation becomes

$$\rho V c \frac{dT_2}{dt} = \frac{T_1 - T_2}{R_2}$$

Because of the energy flows to the elastomer, $\rho V c$ represents the thermal capacitance of the elastomer like $\rho V c = C_2$. Therefore, the differential equation is finally obtained as

$$R_2 C_2 \frac{dT_2}{dt} + T_2 = T_1$$

In order to calculate the thermal capacitance C_2, the density of the elastomer $\rho = 1700 kg/m^3$, the volume of the orange–colored rectangular $V = 0.00265m \times 0.001m \times 0.0072m = 1.908 \times 10^{-8} m^3$, and the specific heat capacity of the elastomer $c = 1175 J/kg \cdot K$ are applied, therefore

$$C_2 = \rho V c = 1700 \times (1.908 \times 10^{-8}) \times 1175 = 0.0381 J/K$$

Also, the thermal resistance of the elastomer R_2 can be calculated with the thermal conductivity $k_2 = 1.2W/m \cdot K$, the cross–sectional area $A = 0.0072m \times 0.001m = 7.2 \times 10^{-6}m^2$, and the length $L_2 = 0.00265m$,

$$R_2 = \frac{0.00265}{1.2 \times (7.2 \times 10^{-6})} = 306.71Ks/J$$

Applying $C_2 = 0.0381J/K$ and $R_2 = 306.71Ks/J$, the differential equation is clarified like following.

$$11.685651s \times \frac{dT_2}{dt} + T_2 = T_1$$

The equation can be once more clarified for the temperature of near the metal's surface T_2 such as

$$T_2(t) = T_1 - constant \times e^{-0.08557504 \times t}$$

.

From the above equation, the initial temperature of T_2 needs to be the room temperature 25°C whatsoever the temperature of the heater T_1 will be at the initial time $t = 0s$. Let's have an example that $T_1 = 75$°C and $T_2 = 25$°C at $t = 0s$. Then, the constant can be calculated like $T_2 - T_1 = 25 - 75 = -50$. Therefore, the equation in this case becomes

$$T_2(t) = 75°\text{C} - 50 \times e^{-0.08557504 \times t}$$

With the time period from $0s$ to $160s$, the thermal analysis of T_2 shows the plot of the red colored curve. The analysis result is approaching to the target temperature with very steep slope and it does not show very accurate tendency on the simulation result and the real experimental measurement. However, there were few factors to be considered such that this calculation just assumed to have only one heater like the hot end resistor and the thermal properties of the materials would be inaccurate when compared to the materials used in real. Nonetheless, it is a meaningful process to establish the thermal modeling and to derive the differential equations.

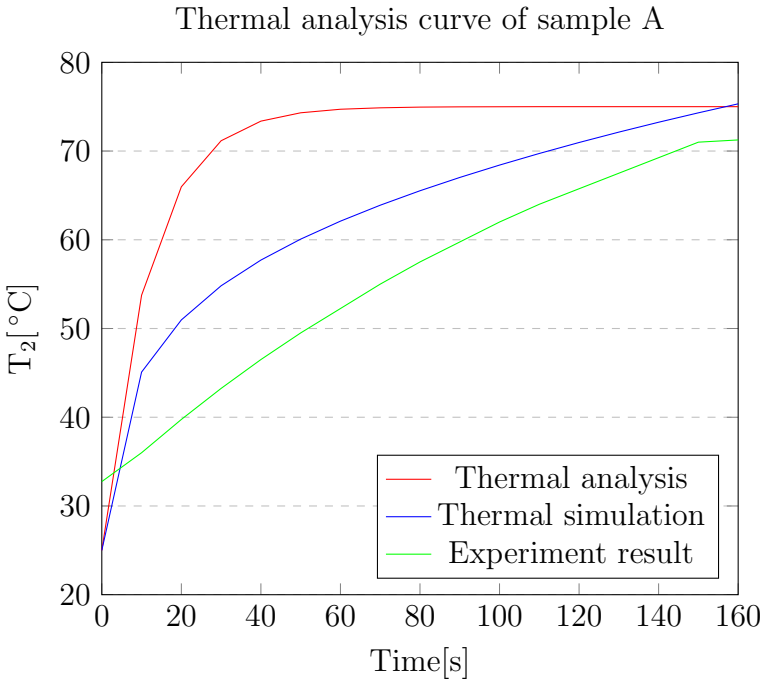

5.3 Thermal Simulation Using Solidworks FEA

Beside of the thermal calculation, the thermal simulation was conducted to find out the transient behavior over time and also figure out whether the simulation will be matched with the experiment curve. Although the thermal conductivity of elastomer was reported as $1.2W/mK$, it was varied and applied to iterate the simulation and find the good matching curve. The sample device was designed as shown in Figure 5.5 and the Ni-Cr wiring was replaced with the plate type instead of the real one due to the complexity of the Ni-Cr wiring design. However, the heat power was used the same value $8.6watt$. Also, the heat power of the hot end resistors was applied totally $6.99watt$. The purpose of this simulation is to compare the fluctuation of the rate of the temperature from 50 °C to 70 °C by the heat power on and off.

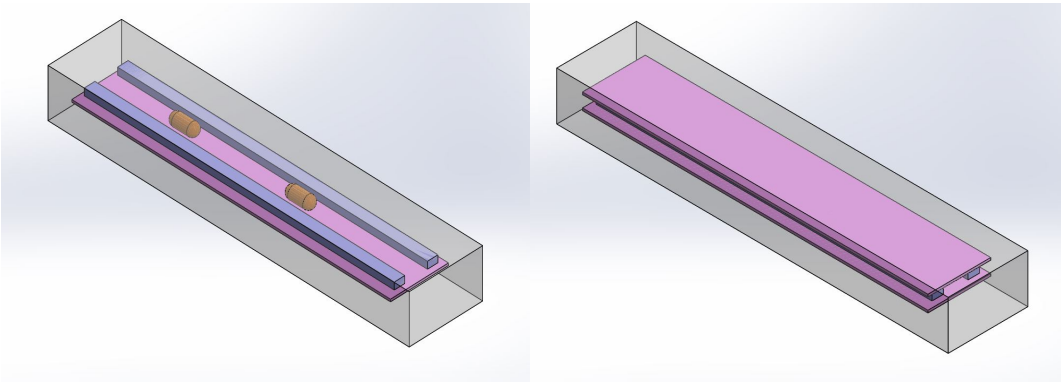

Figure 5.5: Model design of sample A(left) and B(right)

5.3.1 *Simulation to Increase the Temperature to 70 °C*

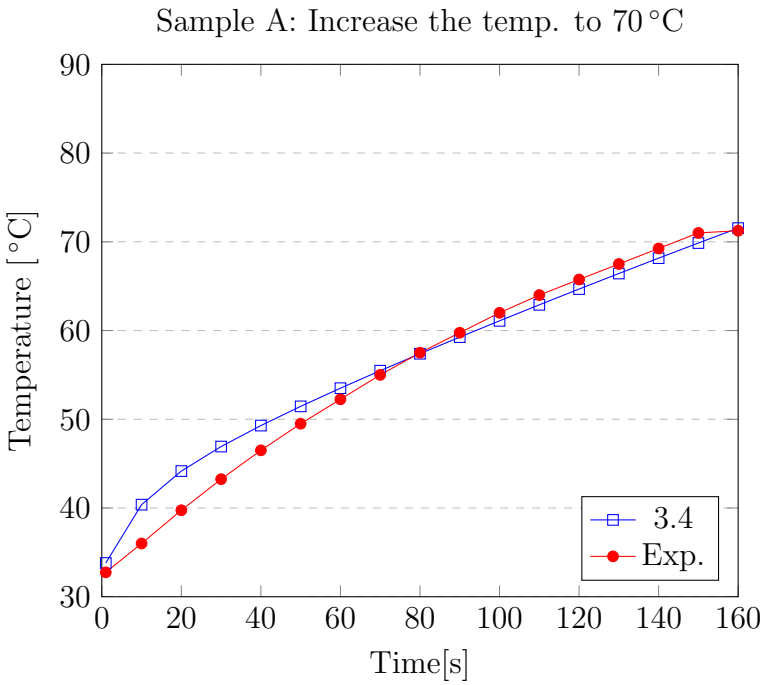

This is the first plot of increasing temperature for sample A which has the hot end resistors and one Ni-Cr layer. The total time lapse was applied with $160s$ when the real sample was reached to 70 °C. The initial temperature was set up with 32 °C being measured as the starting value of the real experiment. The simulation curve was almost matched with the experiment curve when the thermal conductivity of elastomer was set to $3.4W/mK$. At the beginning of the curve, it observed somewhat steeper increase than the experimental one (red color).

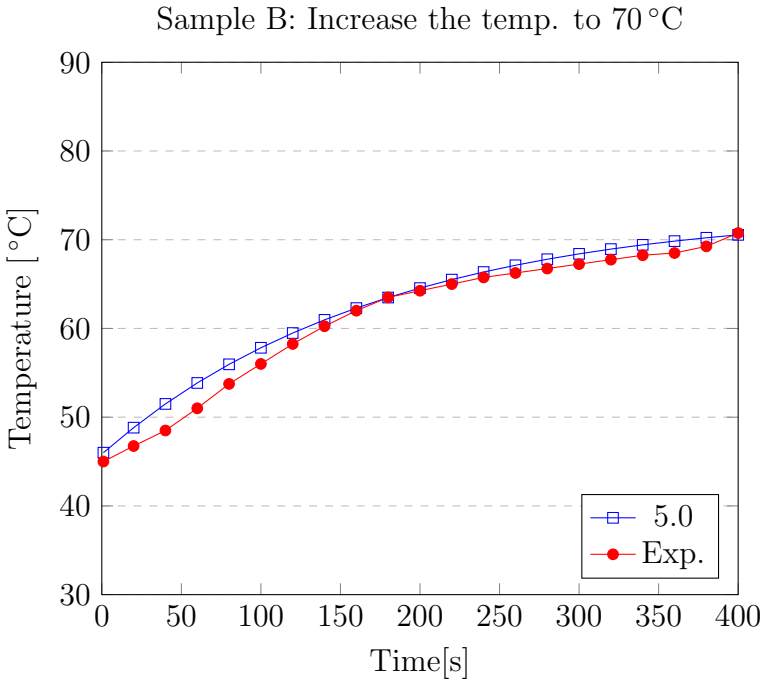

In the case of sample B, it should have applied with much more time like $400s$ than sample A to get reached 70 °C from the room temperature. When sample B was simulated with the same thermal conductivity value of sample A, the rate of temperature in the simulation was observed with much higher than the experiment curve because of the long simulation time period and different heating method such as the Ni-Cr plates. After iterating the simulation with various values of the thermal conductivity, it was finally shown matched like above with the value of $5.0W/mK$.

5.3.2 *Simulation to Decrease the Temperature to* 50 °C

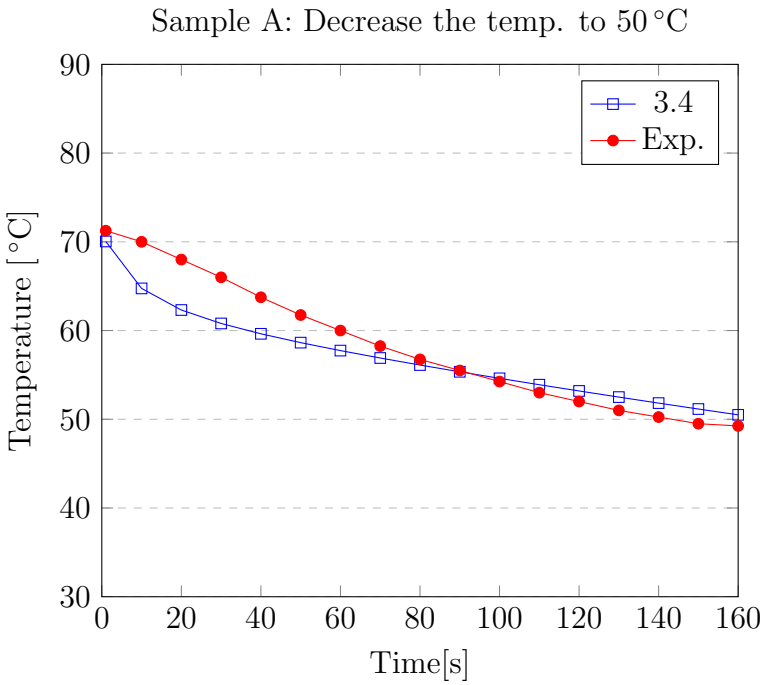

After increasing the temperature for 160s with the heat powers of both resistors and Ni-Cr plate, the thermal loads were turned off and it was simulated to know the decreasing rate of the temperature for another 160s set-up because the cooling time from 70 °C to 50 °C was taken with 160s in the experiment. The previous thermal study by the program was connected to this second simulation, so the initial temperature was set to start from the highest temperature of the first increasing case. As shown in the above plot, it showed a tendency to decrease a little bit steep at the beginning and followed the experiment curve.

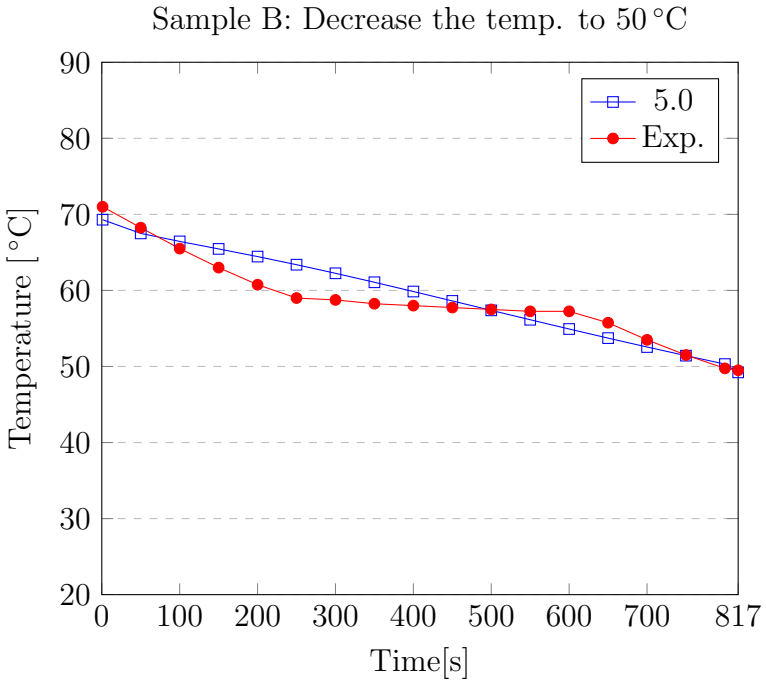

For sample B, the simulation was done with the thermal loads off and applied with the time of 817s taken for cooling down to 50 °C in the experiment. The simulation showed that the temperature was uniformly decreased. On the other hand, the experiment curve started a little bit steeper rate of the temperature change than the simulation at the beginning and showed the different curve in the middle from 60 °C to 55 °C. The intermediate different temperature change is regarded as the transition from the liquid to the solid state.

5.3.3 *Simulation to Increase the Temperature to 70 °C Again*

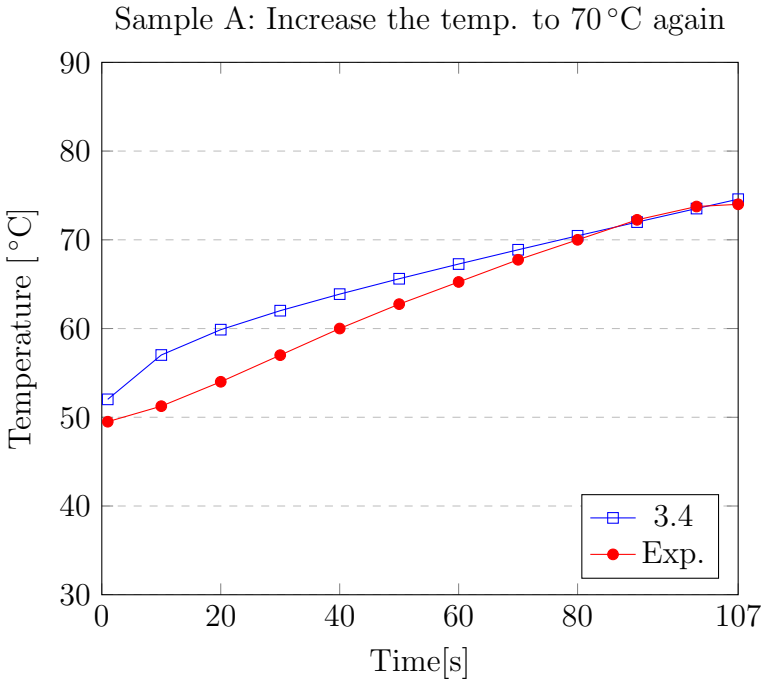

For the second cycle of sample A, the thermal loads were turned on again and it simulated for 107s taken in the experiment to reach 70 °C. The reason why shorter time was taken might be that some heat still existed inside the sample after cooling down to 50 °C in the experiment. For the second temperature increase, as well, it was connected from the previous cooling down study in order to keep the continuous temperature fluctuation. As seen on plot, the simulation curve started with some gap from the experiment curve but was eventually finalized with the match.

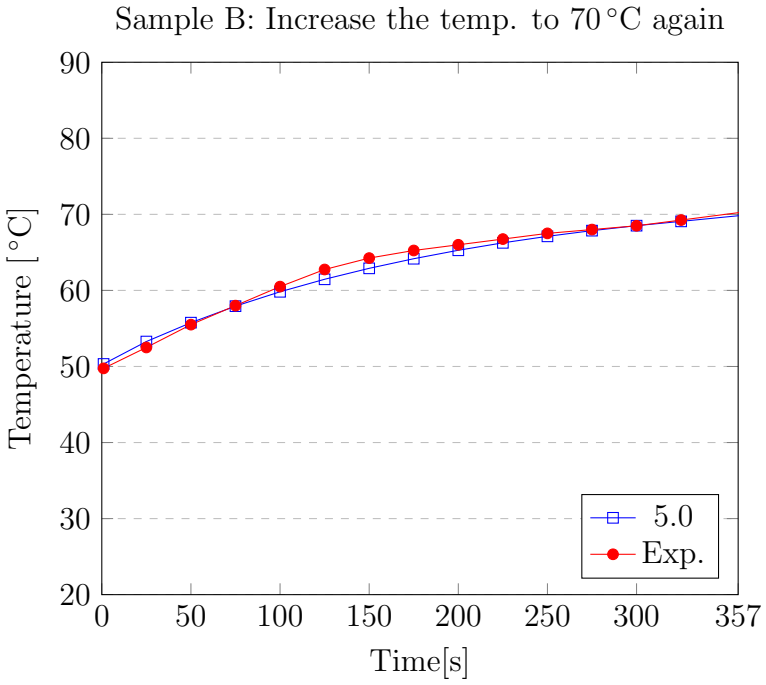

This is also the second temperature increase for sample B and as seen in above, it showed very good matching between the simulation and the experiment curve with the thermal conductivity of elastomer $5.0 W/mK$. It was also connected to the previous simulation and the initial temperature was set up with the lowest one of the first decreasing case. The simulation time was applied with $357s$ as the experiment was taken.

5.3.4 *Simulation to Decrease the Temperature to* 50 °C *Again*

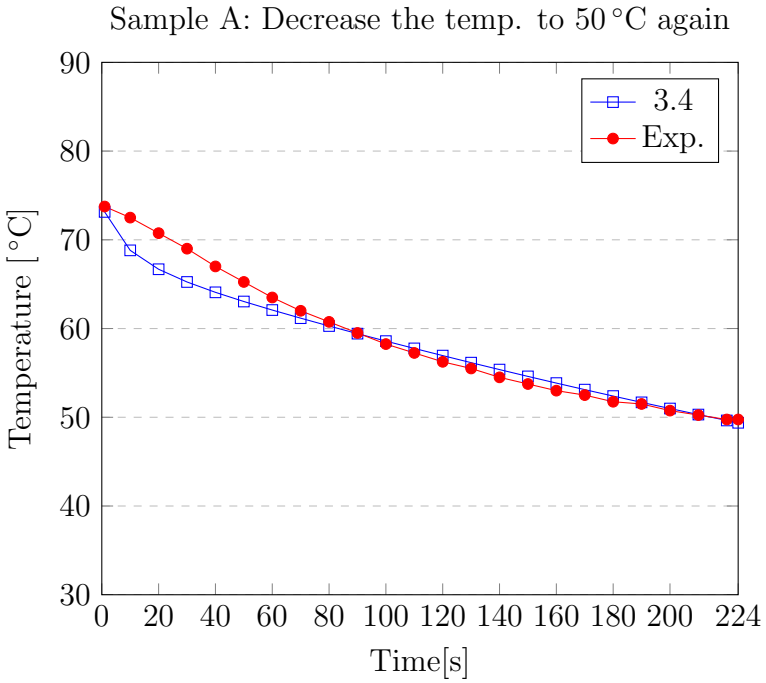

After reaching 70 °C in the second increase, the thermal loads were turned off again and cooled down the device during the time of 224s because it was measured with the same time period to decrease from 70 °C to 50 °C in the experiment. Also, the simulation was connected to the previous thermal study of the second increase for the continuous temperature fluctuation. The plot started with a little bit difference but soon followed the experiment curve over time as shown above.

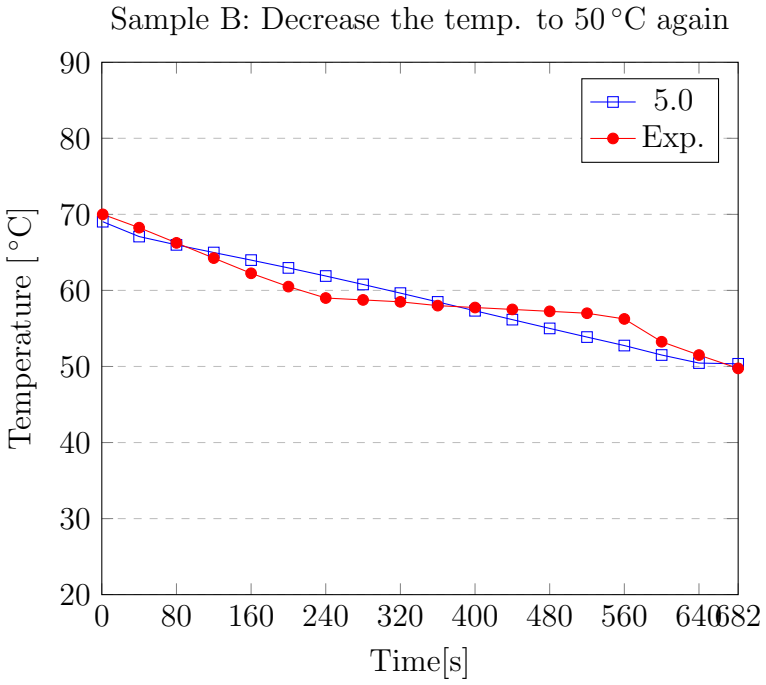

This is the second decrease of sample B that turned off all thermal loads again. In this simulation, it was done for $682s$ of the time when this process of cooling down was taken in the experiment. The tendency of simulation curve was similar to the first decreasing case which fell down evenly. The experiment curve had three steps in the cooling process and the different curve in the middle is also regarded as the transition process of the Field's metal state.

5.3.5 *Simulation vs. Experiment*

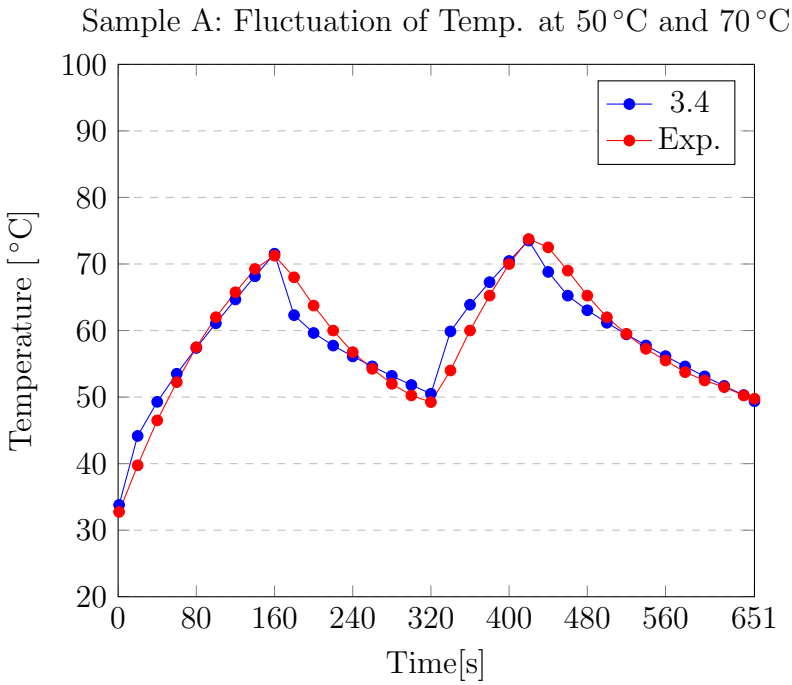

Lastly, the simulation results of each heating and cooling process for sample A were integrated and presented as one curve. In the experiment, the heating sources were powered on and off electrically in order to observe how fast the temperature could go up and down with the specific range of 50 °C and 70 °C. This way of switching on and off was also used in the simulation. As the result of it, when the thermal conductivity of the elastomer was set to $3.4 W/mK$, it showed that the simulation of sample A well followed the experiment curve in the fluctuation.

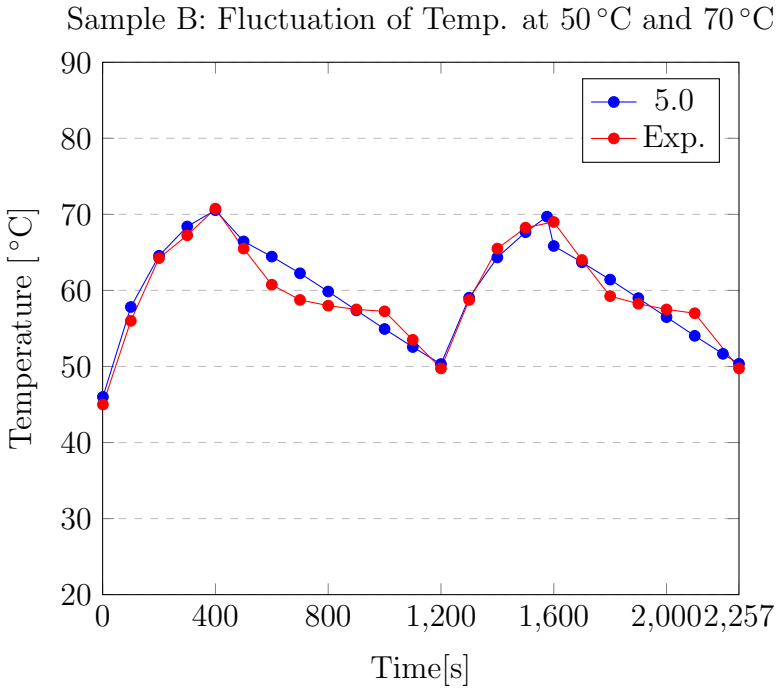

As well, each simulation curve of the increasing and decreasing case for sample B was integrated and presented as seen above. The simulation curve showed the good match with the experiment curve when the thermal conductivity of the elastomer was set to $5.0 W/mK$. One reason for the different thermal conductivity value from sample A would be that sample B had a different heating method like two Ni-Cr plates above and below the Field's metal rods in 3D modeling. Another reason would be that the simulation of sample B was applied with much longer time than sample A as well as the experiment. The evenly decreasing curve in the simulation would be caused by that Solidworks FEA does not take into account the phase change of material.

CHAPTER 6. ADDITIONAL GEOMETRIC COMPLEXITY OF THE METAL SKELETON

The idea of using the low melting point metal, the various shape of the heating element, and manipulation by the tendon can be expanded to the more complex skeletal structure in order to make the device's motion more degrees of freedom.

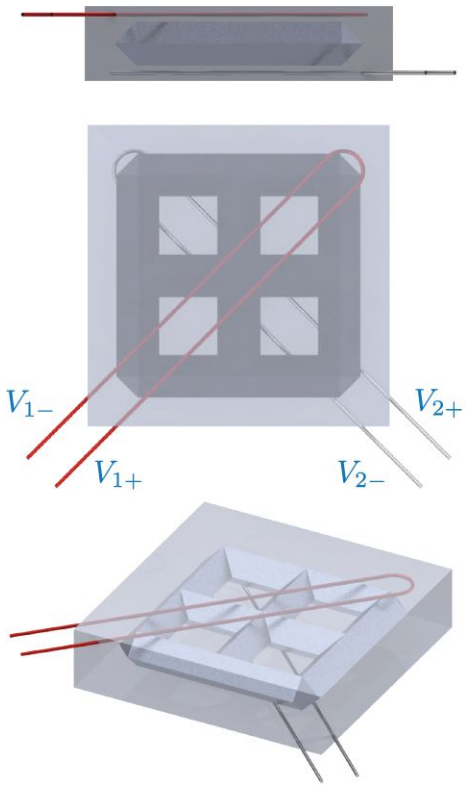

Figure 6.1: More complex skeletal structure like lattice

As shown in Figure 6.1, the Field's metal can be shaped such as "lattice" and it can be melted locally by the thin Ni-Cr wire crossing each other positioned above and bottom layer. The lattice skeleton is encased in the silicone rubber and let's assume that one end can be attached to the wall. When the tip force is applied on the other end, the device with the lattice skeleton and separate heating lines can be bent along with the melted part A, B or C as shown in Figure 6.2.

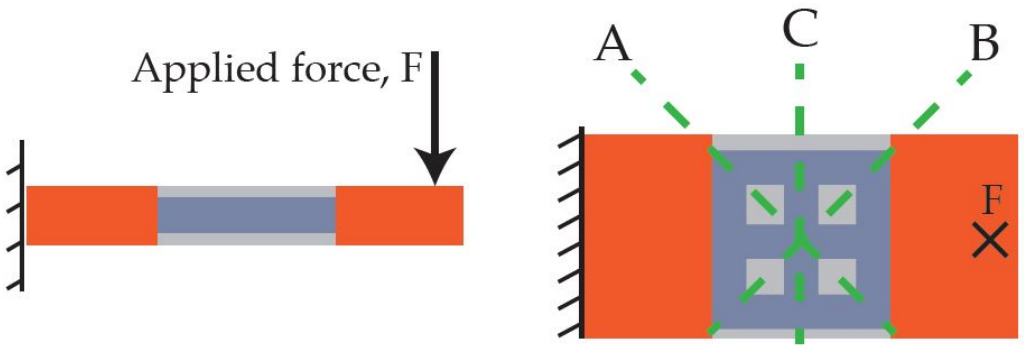

Figure 6.2: Bending moment according to the local heating lines

In order to fabricate the sample, in reality, the mold to secure the Field's metal needs to be designed and manufactured by the 3d printer. The mold is connected internally by the holes for making metal with the lattice pattern and the material of the mold is "High Impact Polystyrene (HIPS)" filament which can be dissolved slowly if immersed in "d-Limonene". As shown in Figure 6.3, the molten Field's metal can be pushed by a syringe into one of the openings of the completed mold. Then, the

mold body is supposed to be dissolved by d-Limonene while putting in the beaker. After removing the mold completely, the Field's metal skeleton can be washed and encased in another mold with the silicone rubber solution. The red mold was designed to fix the Ni-Cr wire positioned up and down through the very small holes keeping the distance from the metal structure layer by layer. When the silicone rubber is totally secured, then the sample can be obtained as seen in left, Figure 6.4.

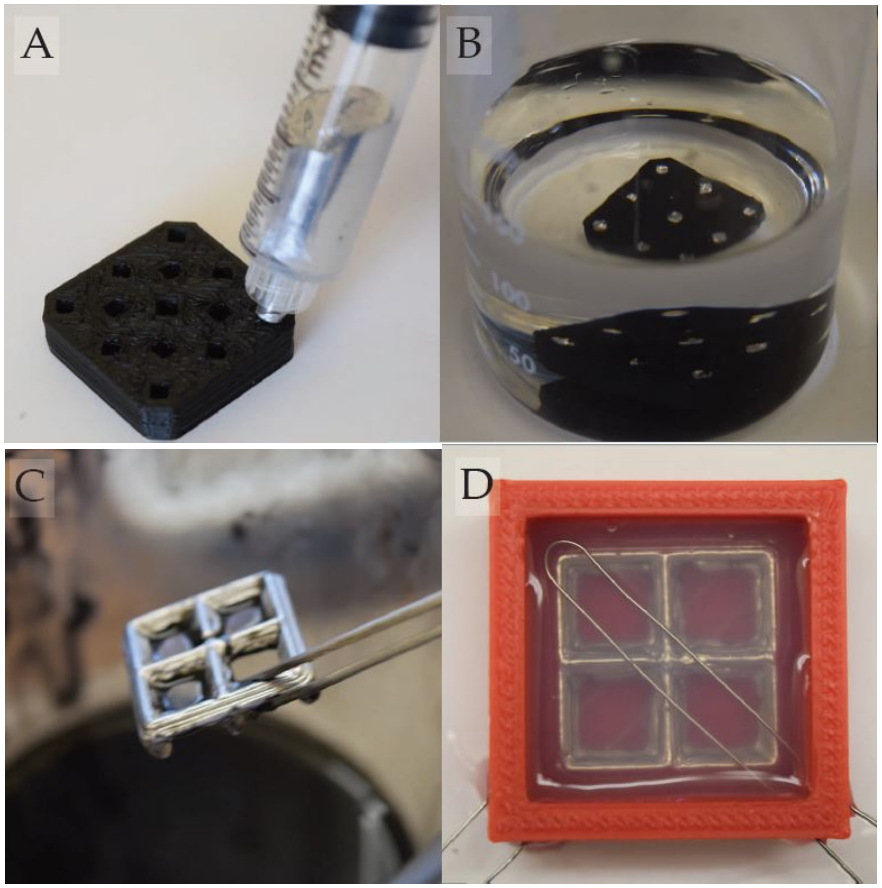

Figure 6.3: Fabrication process of lattice structure sample

Figure 6.4 shows that the flat lattice-shaped Field's metal structure in the rubber can be bent when the only upper Ni-Cr wire was heated. If this unit skeletal structure is connected in series and the heating position can be controlled freely where it is supposed to be melted, the whole device can be manipulated much more degree of freedom. The device can also be applied with the different skeletal structure or another smart material such as "Nitinol alloy" known as the shape memory alloy.

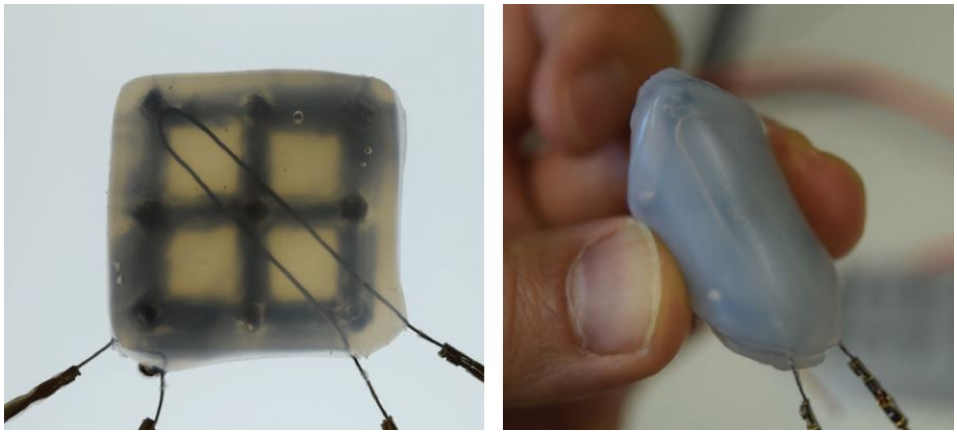

Figure 6.4: Sample of more complex structure and its bending moment

CHAPTER 7. RESULTS AND DISCUSSION

From the experiments of section 4, the first result of increasing to 62 °C for sample A gives that the rate of change of temperature at dual heating elements was faster than single heating element as expected. In comparison between sample A and B, despite using different silicone rubber material, sample A with the power resistors and the Ni-Cr wire was the much faster rate of change than sample B because of higher and more concentrative thermal energy. In order to reach the melting point of 62 °C, sample A took $104s$ with the dual heaters and $292s$ with only Ni-Cr wire respectively, and sample B took $340s$ with both Ni-Cr wires of $8.4watt$ and $827s$ using both Ni-Cr wires with half of the full power, $4.2watt$. The reason why sample A took a little shorter time with only one Ni-Cr wire than sample B with both Ni-Cr wires above and below might be that they didn't use the same rubber material and the difference of each elastomer's thermal conductivity would influence on it.

In the experiment of fluctuation from 50 °C to 70 °C by powered on and off repetitively, sample A showed a much steeper gradient in both increasing and decreasing temperature than sample B. It took approximately $150s$ for both heating and cooling process. On the other hand, sample B consumed more time to raise up to 70 °C and even much more time to lower the temperature 50 °C. This results confirmed

again that the system delivering the high heat intensively from the combination of two resistors and one Ni-Cr wire was more efficient than the system delivering the heat homogeneously from only Ni-Cr wire covering the entire metal rods. As another observation, it was found that the decreasing gradient was slightly changed in the range of 55 °C to 60 °C from the plot of sample B. And it took 400s to reach 70 °C and 800s to go down 50 °C. This phenomenon seems to be the process of material's phase change from the liquid to the solid state and the range is regarded from 55 °C to 60 °C. Also, this phenomenon revealed only sample B while decreasing from 70 °C to 50 °C because sample B had the long time period of the cooling process. On the other hand, sample A couldn't be observed such a phase change because of its much shorter time consumed. The experiment of fluctuation was able to compare the simulation result done by Solidworks FEA. The simulation result of sample A had similar fluctuation tendency compared to the experiment data with the thermal conductivity of elastomer 3.4W/mK. Also, sample B showed a good match with the experiment curve entirely with the thermal conductivity of elastomer 5.0W/mK.

The Field's metal rods are wrapped by the silicone rubber and don't have the direct contact to the heating elements which means that the heat is delivered penetrating through the rubber material. Therefore, the melting point of the metal in this system is thought that it should be compensated to some extent taking into account the thermal resistance of the rubber material between the heat source and the

metal. With this assumption, the plots for finding the liquefied area in section 4.3 showed that both samples were able to bend fully beyond the actual melting point 62 °C. While monitoring the temperature near the metal rod on every second, the experiment to find the appropriate temperature range for bending smoothly was conducted by pulling the tendon carefully and continuously. In the case of sample A, it had natural bending motion at the temperature of around 80 °C. This can also be confirmed by thermal analysis of the steady state behavior in section 5.1. The thermocouple glass braid sensor was laid between the resistor and the Field's metal rod. From the thermal calculation, when the temperature between the resistor's surface $T_3 = 87\,^{\circ}\mathrm{C}$ and the metal's surface $T_4 = 71.4\,^{\circ}\mathrm{C}$ is around 80 °C, then the temperature of metal's outer surface, T_5 becomes 69.5 °C which is fulfilled with the actual melting point, 62 °C. Therefore, the proper temperature to move the finger device without any problem is concluded that at least it should be increased up to 80 °C. In the case of sample B, it took $600s$ to reach 80 °C and also showed the natural motion of bending at this temperature area. The cooling process of both samples had similar tendency that there was a change of the rate in decreasing the temperature. This change of temperature rate was observed in the range of 60 °C and 55 °C in common. It is assumed that the temperature range might be for the process of turning the liquid state into the solid state. Lastly, as seen in Figure 4.2, the finger devices were tried to bend. With more detailed observation, sample A had a tendency of bending

with a little angle sharply. On the other hand, sample B was bent more roundly.

Although both samples did not connect the servo motor system to drive them, they were tried to pull out by the hand and there was no major difficulty in controlling the finger device when they were well melted globally or locally. Considering the existing other types of flexible fingers, it is thought that the controllability of this finger devices is quite comparable with them.

As lessons learned from the results, first of all, it was realized that the silicone rubber needs to be enough in its viscosity. Otherwise, the device itself will stretch down due to its own weight when the Field's metal rods turn out to the liquid state. Sample B had such a phenomenon because of the low viscosity of the silicone rubber compared to sample A. Secondly, it was not easy to cast the Ni-Cr wire to the winding shape using the Ni-Cr mold while making it perfectly planar because the 26 AWG Ni-Cr wire is too thick to be easily handled. As the result of it, imperfectly planar fabrication and its inclusion into the layer would have given the influence in changing the rate at which the heat diffuses to the low melting point metal. This also caused the uneven silicone layer thickness and affected to create the inconstant distance between the Field's metal rods and Ni-Cr wire. While experimenting, the Field's metal rods were oxidized and eventually fractured after the bending motions. This is thought that the metal rods were not melted unevenly due to this unsophisticated fabrication skill. Also, it was not easy and even so demanding for the thermocouple sensor to

implant near the Field's metal and not to move it while curing the elastomer rubber due to the sensor wire's stiffness. Lastly, handling the silicone compound was not absolutely comfortable because of its sticky feature, especially, combining two cured silicone layers needed the skill to remove air bubbles in the uncured silicone compound used to attach them.

As mentioned, while conducting the experiments, the Field's metal rods had a tendency to oxidize when heated quickly, such as blackening the surface of the metal rods, and this resulted in causing the fracture when the devices were applied the bending moments during the cooling process. This phenomenon is still an ongoing and pressing problem to be addressed in future research as any crack in the metal will cause bending concentration at the point of the fracture even when the metal is hardened.

CHAPTER 8. CONCLUSION

Although there have been many kinds of design and fabrication of robotic finger, this approach of a monolithic, composited device that can exhibit capabilities of both soft robotics and traditional rigid-link robotics has the potential of enhancing the field of soft robotics. The devices are simple to fabricate, and further investigations of the geometry of the composited smart materials are ongoing. In this thesis, we just introduced the very basic form of the finger and conducted simple experiments to identify fabrication techniques and the thermal response of the device. However, this series of processes and its results could lead us a more advanced step and give not only other ideas and inspiration but also problems which should be solved.

The specific improvement includes using the Ni-Cr wires solely as a biasing element to raise the entire device temperature close to the melting point and getting localized melting (e.g. finger joints) through another local heat source, such as power resistors. So, the sum of heat by Ni-Cr wire and resistors would be enough to melt the Field's metal at specific locations. Additionally, a tendon will be incorporated to pull the finger while heating. Tendon-based actuation systems have been successfully used to transmit force/motion in devices in which, because of constraints on inertia and size, it is necessary to place the motors remotely with respect to the joints [26].

This ability to control the stiffness of soft robotic components has the potential to enhance the field of soft robots, thus allowing soft robots to exert large forces on environments when necessary, and to withstand external loads while keeping their shape [27]. By making the finger a variable-stiffness device, the robot hand can grasp a soft object and can manipulate objects easily with high dexterity by adjusting the finger softness [28], while maintaining rigidity after a grasp is attained and the device is cooled.

BIBLIOGRAPHY

[1] W. Wang, H. Rodrigue, and S.-H. Ahn, "*Smart soft composite actuator with shape retention capability using embedded fusible alloy structures*," *Elsevier, Composites Part B: Engineering*, vol. 78, pp. 507–514, 2015.

[2] K. A. Shaikh and C. Liu, "*A Bi-Stable Latchable PDMS Valve Employing Low Melting Temperature Metal Alloys*," *TRANSDUCERS 2007 - 2007 International Solid-State Sensors, Actuators and Microsystems Conference*, pp. 2199–2202, 2007.

[3] I. Filip, M. A. D., S. R. F., C. Xin, and W. G. M., "*Soft Robotics for Chemists*," *Angewandte Chemie International Edition*, vol. 50, no. 8, pp. 1890–1895, 2011.

[4] R. A. Bilodeau, E. L. White, and R. K. Kramer, "*Monolithic fabrication of sensors and actuators in a soft robotic gripper*," pp. 2324–2329, 2015.

[5] S. Wanliang, T. Lu, and C. Majidi, "*Soft-matter composites with electrically tunable elastic rigidity*," *IOP, Smart Materials and Structures*, vol. 22, no. 8, 2013.

[6] G. Tonietti, R. Schiavi, and A. Bicchi, "*Design and Control of a Variable Stiffness Actuator for Safe and Fast Physical Human/Robot Interaction*," pp. 526–531, 2005.

[7] R. Schiavi, G. Grioli, S. Sen, and A. Bicchi, "*VSA-II: a novel prototype of variable stiffness actuator for safe and performing robots interacting with humans*," pp. 2171–2176, 2008.

[8] N. G. Tsagarakis, I. Sardellitti, and D. G. Caldwell, "*A new variable stiffness actuator (CompAct-VSA): Design and modeling*," pp. 378–383, 2011.

[9] S. B. Kim, C. Laschi, and B. Trimmer, "*Soft robotics: a bioinspired evolution in robotics*," vol. 31, pp. 287–294, 2013.

[10] S. Kim, C. Laschi, and B. Trimmer, "*Soft robotics: a bioinspired evolution in robotics*," *Trends in biotechnology*, vol. 31, no. 5, pp. 287–294, 2013.

[11] I. D. Walker and M. W. Hannan, "*A novel 'elephant's trunk' robot*," vol. 2, pp. 410–415, 1999.

[12] M. W. Hannan and I. D. Walker, "*Kinematics and the implementation of an elephant's trunk manipulator and other continuum style robots*," *Journal of Field Robotics*, vol. 20, no. 2, pp. 45–63, 2003.

[13] R. F. Shepherd, F. Ilievski, W. Choi, S. A. Morin, A. A. Stokes, A. D. Mazzeo, X. Chen, M. Wang, and G. M. Whitesides, "*Multigait soft robot*," vol. 108, pp. 401–403, 2011.

[14] W. McMahan, B. Jones, I. Walker, V. Chitrakaran, A. Seshadri, and D. Dawson, "*Robotic manipulators inspired by cephalopod limbs*," *Proceedings of the Canadian Engineering Education Association*, 2011.

[15] M. Calisti, M. Giorelli, G. Levy, B. Mazzolai, B. Hochner, C. Laschi, and P. Dario, "*An octopus-bioinspired solution to movement and manipulation for soft robots*," *Bioinspiration & biomimetics*, vol. 6, no. 3, p. 036002, 2011.

[16] Y.-L. Park, B.-r. Chen, C. Majidi, R. J. Wood, R. Nagpal, and E. Goldfield, "*Active modular elastomer sleeve for soft wearable assistance robots*," in *Intelligent Robots and Systems (IROS), 2012 IEEE/RSJ International Conference on*, pp. 1595–1602, IEEE, 2012.

[17] J.-y. Nagase, S. Wakimoto, T. Satoh, N. Saga, and K. Suzumori, "*Design of a variable-stiffness robotic hand using pneumatic soft rubber actuators*," *Smart Materials and Structures*, vol. 20, no. 10, p. 105015, 2011.

[18] M. C. Yuen, R. A. Bilodeau, and R. K. Kramer, "*Active variable stiffness fibers for multifunctional robotic fabrics*," *IEEE Robotics and Automation Letters*, vol. 1, no. 2, pp. 708–715, 2016.

[19] L. H. Scarborough, C. D. Rahn, and E. C. Smith, "*Fluidic composite tunable vibration isolators*," *Journal of Vibration and Acoustics*, vol. 134, no. 1, p. 011010, 2012.

[20] Y. Yang, Y. Chen, Y. Wei, and Y. Li, "*Novel Design and Three-Dimensional Printing of Variable Stiffness Robotic Grippers*," *Journal of Mechanisms and Robotics*, vol. 8, no. 6, p. 061010, 2016.

[21] V. K. Venkiteswaran and H.-J. Su, "*A Three-Spring Pseudorigid-Body Model for Soft Joints With Significant Elongation Effects*," *Journal of Mechanisms and Robotics*, vol. 8, no. 6, p. 061001, 2016.

[22] T. Hassan, M. Manti, G. Passetti, N. d'Elia, M. Cianchetti, and C. Laschi, "*Design and development of a bio-inspired, under-actuated soft gripper*," pp. 3619–3622, 2015.

[23] M. Manti, T. Hassan, G. Passetti, N. dElia, M. Cianchetti, and C. Laschi, *An Under-Actuated and Adaptable Soft Robotic Gripper*, pp. 64–74. 2015.

[24] L. L. Howell, *Compliant mechanisms*. John Wiley & Sons, 2001.

[25] E. S. Ramin and L. Bei, "*Dynamic systems: modeling and analysis*," vol. 2, pp. 316–326, 1995.

[26] G. Palli, G. Borghesan, and C. Melchiorri, "*Modeling, identification, and control of tendon-based actuation systems*," *IEEE Transactions on Robotics*, vol. 28, no. 2, pp. 277–290, 2012.

[27] J. Shintake, B. Schubert, S. Rosset, H. Shea, and D. Floreano, "*Variable stiffness actuator for soft robotics using dielectric elastomer and low-melting-point alloy*," pp. 1097–1102, 2015.

[28] J.-Y. Nagase, S. Wakimoto, T. Satoh, N. Saga, and K. Suzumori, "*Design of a variable-stiffness robotic hand using pneumatic soft rubber actuators*," *IOP, Smart Materials and Structures*, vol. 20, no. 10, p. 105015, 2011.